

MDPI

Article

Synthesis of New 1,4-Naphthoquinone Fluorosulfate Derivatives and the Study of Their Biological and Electrochemical Properties

Natalia V. Aseeva ^{1,*}, Nadezhda V. Danilenko ², Evgenii V. Plotnikov ³, Elena I. Korotkova ¹, Olga I. Lipskikh ¹, Anna N. Solomonenko ¹, Alina V. Erkovich ¹, Daria D. Eskova ³ and Andrei I. Khlebnikov ^{2,*}

- Engineering School of Natural Resources, Department of Chemical Engineering, National Research Tomsk Polytechnic University, Lenin Avenue, 30, Tomsk 634034, Russia; eikor@mail.ru (E.I.K.); lipskih-olga@yandex.ru (O.I.L.); ans51@tpu.ru (A.N.S.); avg48@tpu.ru (A.V.E.)
- The School of Advanced Manufacturing Technologies, National Research Tomsk Polytechnic University, Lenin Avenue, 30, Tomsk 634034, Russia; nadezhda.dani@gmail.com
- Research School of Chemistry & Applied Biomedical Sciences, National Research Tomsk Polytechnic University, Lenin Avenue, 30, Tomsk 634034, Russia; plotnikov.e@mail.ru (E.V.P.); dde5@tpu.ru (D.D.E.)
- * Correspondence: natali.shkuratova@mail.ru (N.V.A.); aikhl@chem.org.ru (A.I.K.)

Abstract: This study presents the synthesis of new fluorosulfate derivatives of 1,4-naphthoquinone by the SuFEx reaction. Anticancer properties of obtained compounds were studied on PC-3 (prostate adenocarcinoma), SKOV-3 (ovarian cancer), MCF-7 (breast cancer), and Jurkat cell lines. All the studied compounds showed higher cytotoxic effects than Cisplatin. The DFT method was applied to determine the electronic structure characteristics of 1,4-naphthoquinone derivatives associated with cytotoxicity. A method of determination of 2,3-dichloro-1,4-naphthoquinone (NQ), 3-chloro-2-((4-hydroxyphenylamino)-1,4-naphthoquinone (NQ1), and 4-((3-chloro-1,4-naphthoquinon-2-yl)amino)phenyl fluorosulfate (NQS) in a pharmaceutical substance using an impregnated graphite electrode (IMGE) was developed. The morphology of the IMGE surface was studied using scanning electron microscopy (SEM). The electrochemical behavior of NQ, NQ1, and NQS was studied by cyclic voltammetry (CV) in 0.1 M NaClO₄ (96% ethanol solution) at pH 4.0 in a potential range from -1 to +1.2 V. Electrochemical redox mechanisms for the investigated compounds were proposed based on the determining main features of the electrochemical processes. Calibration curves were obtained by linear scan voltammetry in the first derivative mode (LSVFD) with the detection limit (LOD) 7.2×10^{-6} mol·L⁻¹ for NQ, 8×10^{-7} mol·L⁻¹ for NQ1, and 8.6×10^{-8} mol·L⁻¹ for NQS, respectively.

Keywords: 1,4-naphthoquinone fluorosulfate derivatives; SuFEx reaction; anticancer properties; impregnated graphite electrode; voltammetry



Citation: Aseeva, N.V.; Danilenko, N.V.; Plotnikov, E.V.; Korotkova, E.I.; Lipskikh, O.I.; Solomonenko, A.N.; Erkovich, A.V.; Eskova, D.D.; Khlebnikov, A.I. Synthesis of New 1,4-Naphthoquinone Fluorosulfate Derivatives and the Study of Their Biological and Electrochemical Properties. *Int. J. Mol. Sci.* 2024, 25, 12245. https://doi.org/10.3390/ijms252212245

Academic Editor: Bernhard Biersack

Received: 14 October 2024 Revised: 4 November 2024 Accepted: 6 November 2024 Published: 14 November 2024



Copyright: © 2024 by the authors. Licensee MDPI, Basel, Switzerland. This article is an open access article distributed under the terms and conditions of the Creative Commons Attribution (CC BY) license (https://creativecommons.org/licenses/by/4.0/).

1. Introduction

A large number of synthetic and natural organic compounds containing a quinone group in their structure can exhibit various biological activities [1]. Many quinones and their derivatives are used as antituberculosis, antimalarial, antimicrobial, antitumor agents, and fungicides [2–6].

The various types of biological activity of 1,4-naphthoquinones, in most cases, are related to the ability of these compounds to take one or two electrons with the formation of the corresponding anion radical (Q^{-}) and dianion radical hydroquinone (Q^{-2}) , as well as to the acid–base properties of these compounds [7,8]. These intermediates interact with essential cellular molecules such as oxygen, DNA, and proteins, altering their biological activity [9–11].

The introduction of different functional groups into the structure of 1,4-naphthoquinones affects the biological activity of these compounds. For example, the introduction of nitrogen and/or sulfur atoms into the structure of 1,4-naphthoquinone derivatives has been shown

to result in their antifungal, antibacterial, and anticancer activity [12–16]. Since cancer is the second most frequent cause of death in the world, and recent advances in new anticancer agents are very promising, naphthoquinone derivatives are attractive compounds for the development of new anticancer drugs [17,18].

The Sulfur(VI)–Fluoride Exchange (SuFEx) reaction was reported [19] as the next embodiment in the development of Click Chemistry. Nowadays, the SuFEx reaction is successfully used for the synthesis of small molecules, protein labeling, production of polymeric materials, and surface modification [19]. SuFEx click chemistry serves as an effective method for the late-stage functionalization (LSF) of bioactive compounds for rapid diversification of drug-like molecules late in the synthesis process—aiming to enhance both their physical and pharmacokinetic characteristics. Utilizing SO₂F₂, Wu's research team successfully transformed a selection of NIH-approved anticancer drugs into their corresponding fluorosulfate derivatives directly within a 96-well plate [20]. By screening a library of 39 compounds, they identified three aryl fluorosulfates that exhibited improved anticancer activity. Thus, using this reaction, new naphthoquinone derivatives with higher anticancer activity can be obtained.

Therefore, the investigation of biological action mechanisms, as well as the development and synthesis of new compounds with more selective biological activity, requires an understanding of the factors that change the physicochemical properties of quinone systems. The study of the relationship between the redox properties of new compounds and their structure can provide insight for the prediction of 1,4-naphthoquinone (NQ) derivatives' pharmacological activity. The investigation and description of the redox properties of NQ derivatives is of great importance.

There are a sufficient number of electrochemical techniques for the determination of quinone-containing compounds with cytotoxic properties in the literature (Table 1).

Compound	Modified Electrode	Method	Linear Con-Centration Range, μ mol L $^{-1}$	Limit of Detection (LOD), nmol ${\bf L}^{-1}$	Objects	Ref.
	PEDOT:PSS-β-CD- SWCNT-COOH/GCE	DPV	0.006–30	1.8	urine	[21]
	PEDOT-MeOH/GCE	DPV	0.001-10,000	0.3	urine	[22]
Shikonin	GCE	SWV	0.0208-1.82	7.8	herbal drug Gromwell Root	[23]
	MWCNTs/ b-CD/GCE	DPV	0.005–10,000	1.0	urine	[24]
	PDDA-GS/GCE	DPV	0.09472-3.789	315.7	herbal drug Lithosper-mum erythrorhi-zon	[25]
	SMDE	SWV	0.5–10	100	pharmaceuti-cal preparations	[26]
Doxorubicin	multifunctional carbon dots/ magnesi-um oxide (CDs/MgO/SPCE)	CV	0.1–1	90	pharmaceuti-cal preparations	[27]
	p-Ag/SAE	DPCSV DPV	0.6–10 1.0–40	440 840	human urine	[28]
	GQD/GCE	DPV	0.018-3.600	16	human plasma	[29]
Daunorubicin	ds-DNA/Pt/ SWCNTs/GCE	DPV	0.004-250	1.0	pharmaceuti-cal preparations	[30]

Table 1. Electrochemical techniques for the determination of quinone-containing compounds.

However, since the number of newly synthesized biologically active naphthoquinone derivatives is constantly increasing, new analytical techniques need to be developed.

In the present study, the 1,4-naphtoquinone fluorosulfate derivatives were obtained via the SuFEx reaction, which could be used as a tool for functionalization in order to improve both the physicochemical and pharmacokinetic properties of organic compounds.

Anticancer properties of the obtained derivatives were investigated on PC-3 (prostate adenocarcinoma), SKOV-3 (ovarian cancer), MCF-7 (breast cancer), and Jurkat cell lines. An express technique for the quantitative determination of 1,4-naphtoquinone derivatives at the impregnated graphite electrode (IMGE) in a pharmaceutical substance was developed.

Despite the fact that the presented analytical technique is less sensitive compared to the existing methods (Table 1), it can be used for express determination of newly synthesized 1,4-naphtoquinone derivatives. The advantages of using the IMGE in this work are as follows: easy renewal of electrode surface after the adsorption of organic compounds, in contrast to commercial carbon-based electrodes, as well as the absence of expensive and time-consuming modification steps.

2. Results and Discussion

2.1. The Synthesis of Naphthoquinone Derivatives

One of the investigated compounds, 2,3-dichloro-1,4-naphthoquinone (NQ) (with trade names "Dichlone" and "Phygon"), is used as a fungicide for the treatment of fruits, field crops, vegetables, ornamental plants and seeds. Moreover, due to easy accessibility and high stability, NQ is known in modern chemistry as a key synthetic precursor for the synthesis of new 1,4-naphthoquinone derivatives with various types of pharmacological activity [31,32].

Naphthoquinone derivatives could be obtained in a number of different ways. Preparation of 1,4-naphthoquinone derivatives from 2,3-dichloro-1,4-naphthoquinone is one of the common methods that can be found in the literature [17,33]. Using this method, we obtained the naphthoquinone derivatives 3-chloro-2-((4-hydroxyphenyl)amino)-1,4-naphthoquinone (NQ1) and 3-chloro-2-((3-hydroxyphenyl)amino)-1,4-naphthoquinone (NQ2) (Scheme 1), which possess antitumor biological activity [34]. The presence of a hydroxyl group makes it possible to further functionalize these compounds through the SuFEx reaction.

Scheme 1. Synthesis of hydroxyphenylamino derivatives from 2,3-dichloro-1,4-naphthoquinone.

Earlier, the use of the SuFEx reaction for the preparation of 1,4-naphthoquinone derivatives led to new potential trypanocidal prototypes against the *Trypanosoma cruzi* (*T. Cruzi*) parasite [35]. In general, SuFEx click reactions provide a useful tool for obtaining bioactive molecules and their late-stage functionalization (LSF) for quick improvements in both physical and pharmacokinetic properties [20].

It is known that aromatic alcohols react selectively with gaseous SO_2F_2 , leaving aliphatic alcohols, aliphatic and aromatic amines, and carboxylic groups intact [19]. In this view, using the SuFEx reaction between compound NQ1 and SO_2F_2 in the presence of 1,8-diazabicyclo[5.4.0]undec-7-ene (DBU), we obtained 4-((3-chloro-1,4-naphthoquinon-2-yl)amino)phenyl fluorosulfate (NQS) (Scheme 2). The process was carried out in a two-chamber reactor (Figure S1), where gaseous SO_2F_2 was formed in chamber A, while the click reaction proceeded in chamber B.

However, this method gave a very low yield of only 8–9% for compounds **NQS** and **NQS2**. Such yields are not typical for the SuFEx reaction and can be attributed to peculiarities of the naphthoquinone moiety, e.g., to the tendency of naphthoquinones to form stable tautomers [36].

Scheme 2. Synthesis of 1,4-naphthoquinone-based fluorosulfate derivatives.

Taking into account the high reactivity of silyl derivatives in SuFEx reactions [19], we have preliminarily synthesized compounds **NQ1a** and **NQ2a** using *tert*-butyldimethylsilyl chloride (TBSCl) according to Scheme 3.

Scheme 3. Synthesis of the silylated hydroxyphenylamino derivatives.

We further used the silyl derivatives **NQ1a** and **NQ2a** as substrates for the SuFEx reaction, which was conducted under the same conditions as in Scheme 2. The achieved yields of the target products were 95 and 85% for compounds **NQS** and **NQS2**, respectively (Scheme 4).

Scheme 4. Synthesis of fluorosulfates from the silylated derivatives.

We have checked the possibility of performing a one-pot synthesis of the fluorosulfates NQS and NQS2 without the intermediate isolation of the silylated compounds (Scheme 5). Firstly, in chamber B of the reactor, the silylation was carried out, which was controlled by TLC. At the completion of this process, DBU was added to chamber B, while SDI and KF were placed in chamber A of the reactor. The reactor was tightly closed and formic acid was injected through the septum into chamber B to activate the formation of SO_2F_2 gas. The one-pot synthesis led to low yields of 32% (NQS) and 22% (NQS2). Therefore, the isolation of intermediate products NQ1a and NQ2a is the necessary preparative step of the synthesis.

Scheme 5. One-pot synthesis of the 1,4-naphthoquinone-based fluorosulfates.

Thus, we can conclude that the best SuFEx reaction substrates for the synthesis of target naphthoquinone fluorosulfate derivatives are silyl ethers. The reason for this may be the formation of the strong silicon–fluorine bond during the reaction (the Si-F bond dissociation energy is 135 kcal/mol [37]), which easily leads to the formation of the target products.

The spectral and analytical data for the synthesized compounds are given in Materials and Methods. The NMR spectra are shown in Figures S2–S11.

2.2. Biological Activity Study

2.2.1. Evaluation of Biological Activity and ADMET Parameters in Silico

The potential biological activity of the synthesized compounds was established using the computer program PASS (Prediction of Activity Spectra for Substances) [38]. The program allows estimating manifestation of different types of biological activity by the compounds with high accuracy and probability. The data are presented in Table S1, where Pa and Pi values are interpreted as the probabilities of a molecule belonging to the classes of active and inactive compounds, respectively.

According to the PASS data, the investigated naphthoquinones, especially compound **NQ**, may exhibit biological activities against a large number of biotargets. Among them are anticancer effects, which were also discovered previously for different substituted naphthoquinones [39]. Hence, it is reasonable to perform an experimental study of anticancer properties of compounds **NQ**, **NQ1**, **NQ2**, **NQS**, and **NQS2** and evaluate their ADME characteristics.

The ADME properties are necessary in the initial stages of drug development and determine either the bioavailability of a potential drug or its elimination from the study [40]. We assessed the ADME characteristics of compounds NQ, NQ1, NQ2, NQS, and NQS2 using the SwissADME online tool (http://www.swissadme.ch/, accessed on 2 September 2024). According to the results presented in Table 2, the ADME parameters indicate the ability of these five compounds to cross the blood–brain barrier.

Properties	NQ	NQ1	NQS	NQ2	NQS2
Formula	$C_{10}H_4Cl_2O_2$	C ₁₆ H ₁₀ ClNO ₃	C ₁₆ H ₉ ClFNO ₅ S	C ₁₆ H ₁₀ ClNO ₃	C ₁₆ H ₉ ClFNO ₅ S
Molecular weight	227.04	299.71	381.76	299.71	381.76
Number of heavy atoms	14	21	25	21	25
Fraction Csp ³	0.00	0.00	0.00	0.00	0.00
Number of rotatable bonds	0	2	4	2	4
Number of H-bond acceptors	2	3	6	3	6
Number of H-bond donors	0	2	1	2	1
Molar Refractivity	53.84	79.89	88.57	79.89	88.57
tPSA, Å ²	34.14	66.4	97.92	66.4	97.92
Lipophilicity. Consensus Log Po/w	2.55	2.65	2.93	2.65	2.90
BBB permeant	yes	yes	no	yes	no
Synthetic accessibility	2.39	2.79	3.02	2.83	3.10
Bioavailability Score	0.55	0.55	0.55	0.55	0.55
LD ₅₀ mg/kg	160	1260	2000	2000	2000
Toxicity class	3	4	4	4	4

Table 2. ADME, bioavailability and toxicity parameters of selected naphthoquinone derivatives.

We obtained bioavailability radar plots that display drug-likeness scores for the compounds. Six important physicochemical properties were considered, including lipophilicity, molecular size, polarity, solubility, conformational flexibility, and insaturation [41]. The naphthoquinone derivatives studied were found to have generally satisfactory ADME properties, with graphs indicating high bioavailability (Figure 1).



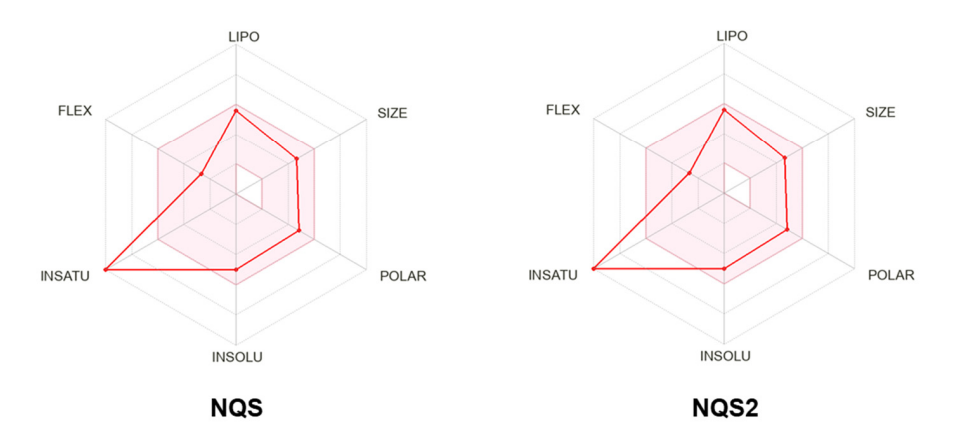


Figure 1. Radar bioavailability plots for compounds **NQ**, **NQ1**, **NQ2**, **NQS**, **NQS2**. The plots show the parameters LIPO (lipophilicity), SIZE (molecular weight), POLAR (polarity), INSOLU (insolubility), INSATU (insaturation) and FLEX (conformational flexibility).

The potential toxicity of the synthesized compounds was established using the Prediction Of Toxicity Of Chemicals (ProTox 3.0) software available online (https://tox.charite.de/protox3/, accessed on 25 August 2024). In silico toxicity assessment showed that compounds NQ1, NQ2, NQS, and NQS2 belong to toxicity class 4 (Table 2), while compound NQ belongs to class 3 ($LD_{50} = 160 \text{ mg/kg}$). It should be noted that fluorosulfate derivatives NQS, NQS2 have a higher LD_{50} value; therefore, they are less toxic.

Based on the calculated ADME parameters, LD₅₀ values (Table 3), and bioavailability radars (Figure 1), the compounds are expected to have good bioavailability and low toxicity.

Table 3. Results of the experimental determination of the half inhibitory concentration (IC₅₀ in μ M) for the cancer cell lines (n = 6).

Cell Line	NQ	NQ1	NQ2	NQS	NQS2	Cisplatin
PC-3	22.31 ± 3.54	1.59 ± 0.10	0.9 ± 0.07	6.23 ± 1.08	2.60 ± 0.30	40.89 ± 6.20
MCF-7	9.89 ± 1.03	7.68 ± 0.62	4.38 ± 0.48	17.48 ± 3.02	5.44 ± 0.89	33.46 ± 5.42
SKOV-3	20.56 ± 2.16	5.98 ± 0.65	2.19 ± 0.32	7.22 ± 0.92	3.95 ± 0.42	32.81 ± 7.12
Jurkat	37.88 ± 5.49	2.87 ± 0.10	1.77 ± 0.18	4.24 ± 0.34	3.06 ± 0.36	19.97 ± 1.98

2.2.2. The Cytotoxicity Study

It was shown in [42] that sulfur-containing naphthoquinone derivatives showed the greatest activity against the PC-3 prostate cancer cell line. Therefore, the resulting compounds were tested for cytotoxicity (MTT, microscopy) against different cancer cell lines, including PC-3 prostate cancer (Table 3).

A pronounced cytotoxic effect was shown for all the studied compounds (Table 3). Inhibition of tumor cell growth by the investigated naphthoquinones significantly exceeded the effects of the standard cytostatic agent cisplatin. The prostate cancer (PC-3) and lymphoblastic leukemia (Jurkat) cell lines were more susceptible to the effects of the compounds; however, in general, the revealed trends were observed in all studied cell lines. Pairwise comparison of cytotoxicity parameters of compounds NQ1 and NQS, NQ2 and NQS2, respectively, allow us to conclude that compounds NQ1 and NQ2 have a slightly higher inhibitory effect on all the studied cell lines in comparison with their fluorosulfate containing analogues. In general, the cytotoxicity parameters of both groups are close. On the other hand, all the modified compounds were found to be significantly superior in cytotoxic effect to the unmodified NQ precursor. At the same time, the fluorosulfate group allows modified molecules to be grafted to the surface of materials [43]. This provides a fundamental basis for the development of new hybrid biomaterials.

The breast cancer (MCF-7) cells proved to be relatively more resistant to the effects of all compounds. However, the compounds **NQ2** and **NQS2** showed high cytotoxicity on it; the IC $_{50}$ value was in the range of 4–5 μ M, whereas for cisplatin, the IC $_{50}$ was 33.5 μ M.

Cell death variants (apoptosis of different stages and necrosis) were assessed on the Jurkat cell line (Figure 2). A dose-dependent increase in the level of cell death was revealed, with apoptosis induction being the main mechanism of this process. The proportion of primary necrotic cells remained low even when exposed to the maximum concentrations of the substances used. The obtained data correlate well with cytotoxicity parameters of studied compounds on other tumor lines.

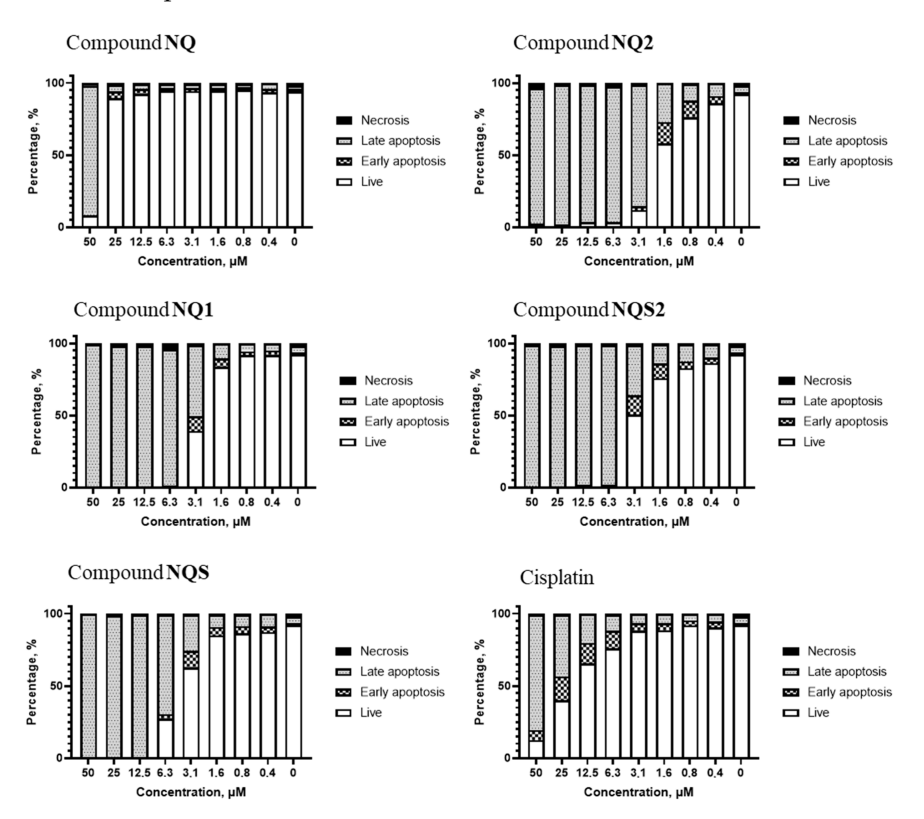


Figure 2. Distribution of cell death variants in the Jurkat cell population after 24 h of exposure to compounds at different concentrations (n = 6). The ratio of viable cells to cells in a state of early apoptosis, late apoptosis or necrosis is shown in the graphs.

Massive induction of apoptosis in cell culture is caused by critical unrepairable cell damage after xenobiotic exposure and is usually accompanied by pronounced mitochondrial dysfunction, leading to oxidative stress. This phenomenon was shown by evaluating the level of reactive oxygen species production in cells under the influence of the studied substances (Figure 3).

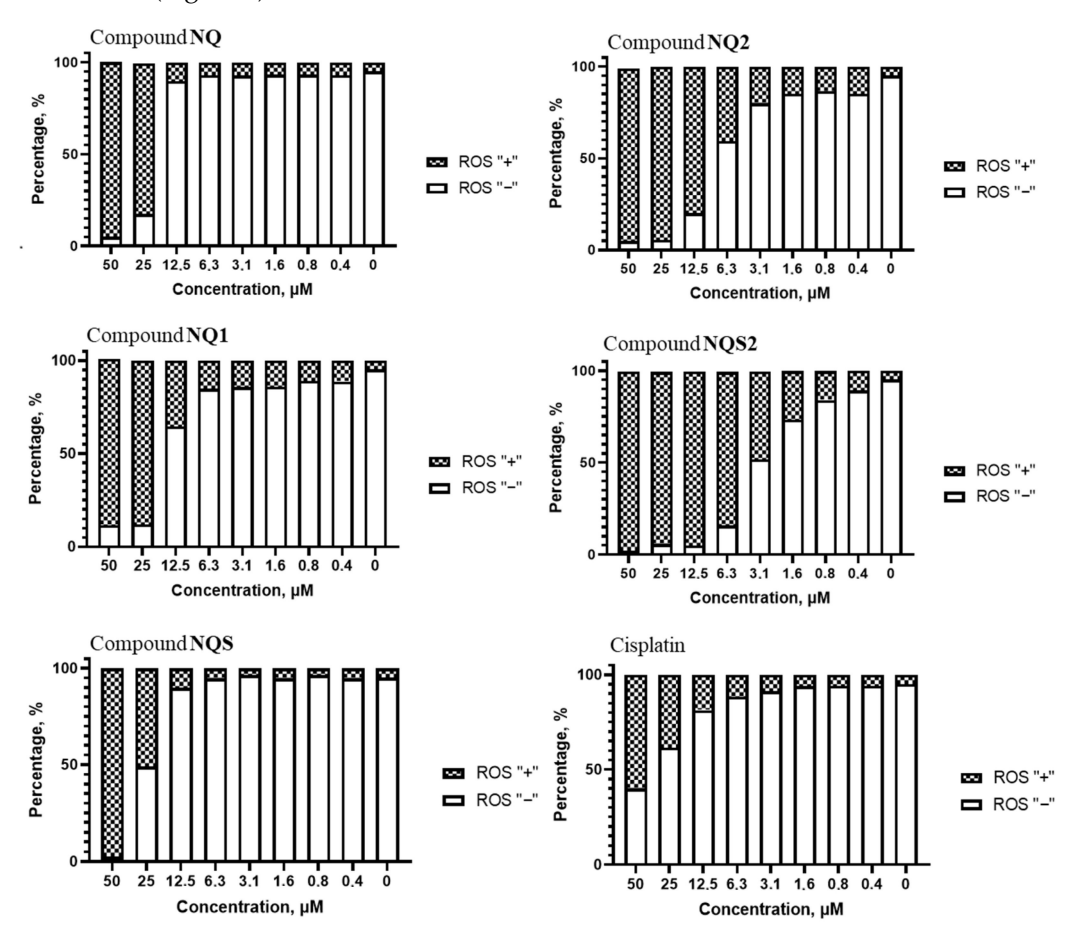


Figure 3. Oxidative stress level in Jurkat cells after 24 h of exposure to compounds at different concentrations. Results are shown as the percentage of cells with high levels of reactive oxygen species production (ROS+) and ROS-negative cells (ROS-) from the total cell population (n = 6).

The level of oxidative stress in cells (the level of ROS production) also correlates with an increase in the concentration of substances (Figure 2). The highest level of induction of oxidative stress in cells was found under the influence of compounds **NQ2** and **NQS2**, which significantly exceeds the standard cytostatic cisplatin in this indicator.

Upon evaluation of the cytotoxic potential of the investigated compounds, **NQ1**, **NQ2**, **NQS**, and **NQS2** demonstrated significant antiproliferative effects across the tested tumor cell lines. The observed cytotoxicity was concomitant with a critical elevation in intracellular oxidative stress parameters and an augmentation of apoptotic markers.

While the cytotoxic response exhibited variability among different tumor cell types, a consistent dose-dependent trend was observed across all experimental cell cultures. This heterogeneity in cell sensitivity may be attributed to the intrinsic differences in cellular redox homeostasis, apoptotic machinery, and drug efflux mechanisms among the diverse neoplastic cell types.

The mechanistic underpinnings of the observed effects suggest that these compounds may act as a redox disrupter, potentially interfering with mitochondrial electron transport and/or inducing the generation of reactive oxygen species. The consequent oxidative stress triggers apoptotic cascades, as evidenced by the increased markers of programmed cell death.

2.2.3. The Electronic Structure of Naphthoquinones in Relation to Cytotoxicity

In this work, we performed quantum chemical calculations using the DFT method for a group of naphthoquinone derivatives to determine the characteristics of their electronic structure related to cytotoxicity. The calculations were carried out using the ORCA 4.2 program. Geometry optimization was performed using the BP86 functional and the triple-zeta basis set def2-TZVPP. Dispersion interactions were accounted for using the D3BJ approximation. This level of theory, according to the literature, provides a good degree of accuracy for the geometry of organic molecules and intermediates [44]. Subsequently, for each compound, calculations were performed without further geometry optimization (single point) using the ω B97X-D3 functional and the 6-311++G(3df,3pd) basis set to obtain more accurate results for orbital energies [45].

For further analysis, we selected the following characteristics of the electronic structure: the energy of the highest occupied molecular orbital [E(HOMO)], the energy of the lowest unoccupied molecular orbital [E(LUMO)], vertical electron affinity (VEA), absolute hardness η , absolute electronegativity χ , and the reactivity index ω . The values of η , χ , and ω were calculated using the equations:

$$\eta = [E(LUMO) - E(HOMO)]/2 \tag{1}$$

$$\chi = -[E(LUMO) + E(HOMO)]/2$$
 (2)

$$\omega = \chi^2 / (2\eta) \tag{3}$$

We have found that the energies of frontier molecular orbitals and the related characteristics of the electronic structures of the investigated naphthoquinones (Table S2) are tightly correlated with IC_{50} values for some of the cancer cell lines (Table 4), with the exception of MCF-7 cells.

Table 4. The Pearson correlation coefficients between the cytotoxicity (IC $_{50}$) and the electronic structure characteristics of the investigated naphthoquinone derivatives*.

	E(HOMO) (eV)	E(LUMO) (eV)	VEA (kcal/mol)	η (eV)	χ (eV)	ω (eV)
PC-3	-0.96	-0.90	0.77	0.96	0.96	0.93
MCF-7	-0.24	-0.55	0.64	0.14	0.31	0.44
SKOV-3	-0.91	-0.84	0.70	0.90	0.90	0.88
Jurkat	-0.94	-0.81	0.66	0.96	0.92	0.87

^{*} The significant correlation coefficients (p < 0.05) are highlighted in bold. The statistical significance was determined using the STATISTICA (Version 6) software.

Thus, the positive correlations with absolute hardness η and electronegativity χ show that an increase in these values leads to higher IC₅₀, i.e., to lower cytotoxicity with respect to PC-3, SKOV-3, and Jurkat cells. The opposite is true for the E(HOMO) values. According to the correlation data, an increase in the HOMO energy leads to higher cytotoxic activities of the investigated naphthoquinones. The same applies to E(LUMO), although in this case, a significant correlation was obtained only for the PC-3 cells. In general, the DFT results indicate that lower electrophilicity of the compounds would be favorable for the cytotoxic activity.

2.3. Electrochemistry

2.3.1. Electrochemical Behavior of NQ, NQ1 and NQS at IMGE

The manifestation of biological activity by naphthoquinones is largely due to their oxidation–reduction properties and processes with electron transfer [46]. In this regard, we carried out a study of the electrochemical behavior of naphthoquinones **NQ**, **NQ1**, and **NQS**. Moreover, using IMGE, it is possible to develop methods for the analysis of biologically active naphthoquinones.

The electrochemical behavior of NQ, NQ1, and NQS was studied by cyclic voltammetry (CV) in $0.1 \, \text{M} \, \text{NaClO}_4$ 96% ethanol solution with the addition of HCl to pH 4.0 in a potential range from -1 to $+1.2 \, \text{V}$. The analyzed solution contained $0.2 \, \text{mmol} \cdot \text{L}^{-1}$ of the investigated compounds. Figure 4 shows that NQ, NQ1 and NQS give a pair of peaks caused by the electrochemical reaction of the quinone group. The introduction of different substituents to the NQ structure leads to a shift of the peaks toward more positive values (NQ1 and NQS). Moreover, for NQ1 and NQS, we can note the presence of an additional pair of peaks due to the electrochemical redox reaction of the imino group and one peak (NQ1) provided by the electrooxidation of the hydroxyl group.

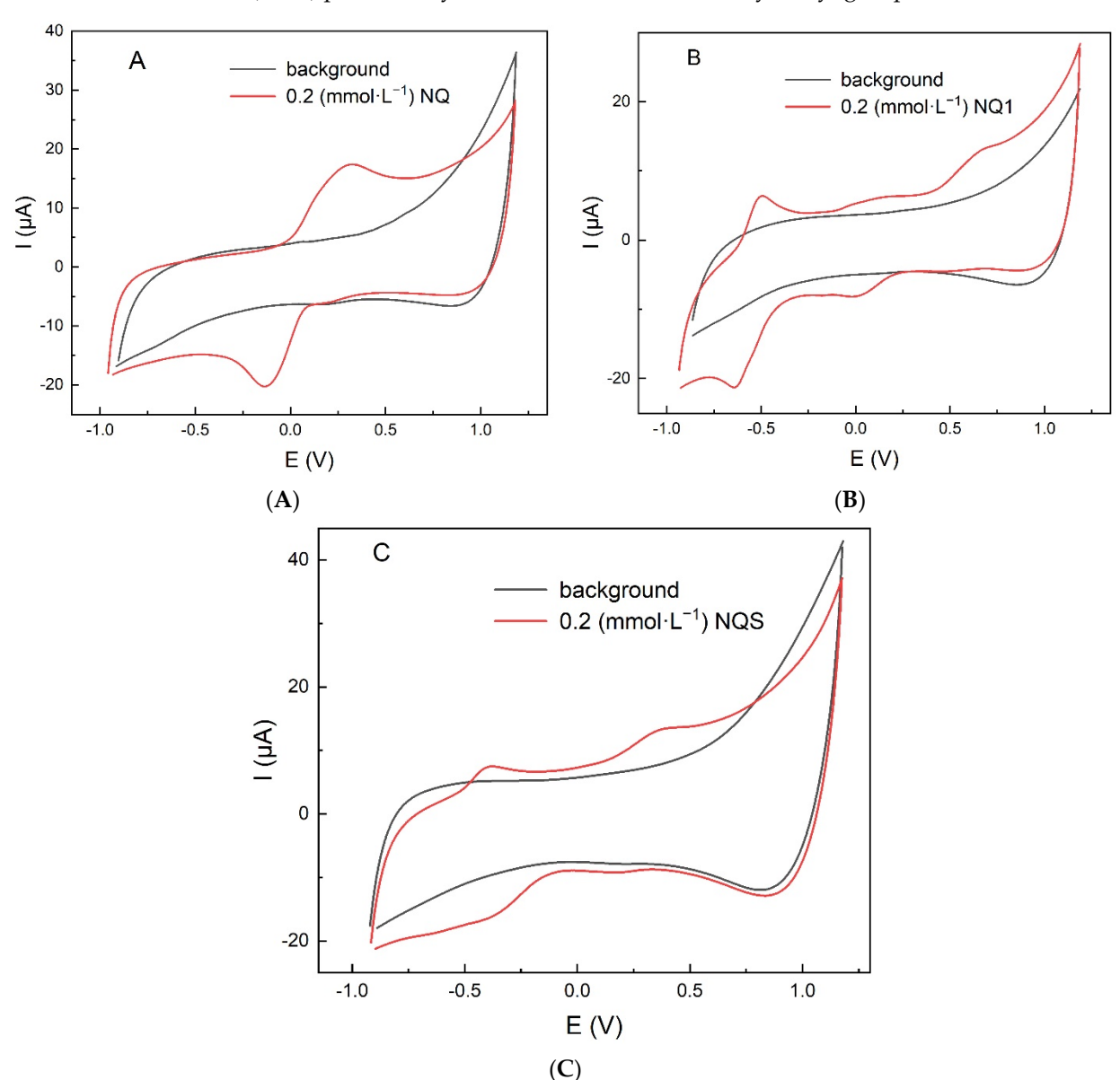


Figure 4. Cyclic voltammograms: **(A)** NQ, **(B)** NQ1, **(C)** NQS in 0.1 M NaClO₄ 96% ethanol solution (pH 4.0) at the IMGE vs. silver chloride electrode (1 mol·L $^{-1}$ KCl); v = 100 mV·s $^{-1}$.

Table 5 shows the values of the anodic and cathodic peak potentials of the investigated 1,4-naphthoquinone derivatives and their relation with the functional groups.

The cathodic peak corresponding to the quinone group (NQ) and the anodic and cathodic peaks corresponding to the imino group (NQ1 and NQS, respectively) were chosen as analytical signals to develop a voltammetric technique for the determination of the compounds.

Compound	Functional Group	E _{pa} , V	E _{pc} , V
NQ	Quinone	0.26 ± 0.05	-0.13 ± 0.05
NQ1	Imino Quinoid Hydroxyl	-0.51 ± 0.05 0.64 ± 0.05 0.14 ± 0.05	$-0.65 \pm 0.05 \ 0.03 \pm 0.05 \ ext{no signal}$
NQS	Imino Quinone	-0.41 ± 0.05 0.36 ± 0.05	-0.36 ± 0.05 0.18 ± 0.05

Table 5. Potentials of the anodic and cathodic peaks of the investigated 1,4-naphthoquinone derivatives.

Two main criteria were applied to confirm the adsorption nature of the electrochemical process. The dependence of the peak current on the potential scan rate should be linear, and the value of the Semerano criterion for the logarithmic dependence of the peak current on the potential scan rate should be greater than 0.5 [47].

As can be seen from Figure 5, for compounds NQ and NQ1, the dependence of the peak current on the scanning potential rate is linear, whereas for compound NQS, this dependence is nonlinear. The values of the Semerano criterion are 0.64, 0.57, and 0.52 for compounds NQ, NQ1, and NQS, respectively. Based on the obtained data, the electrochemical processes for the analyzed compounds were of an adsorption nature.

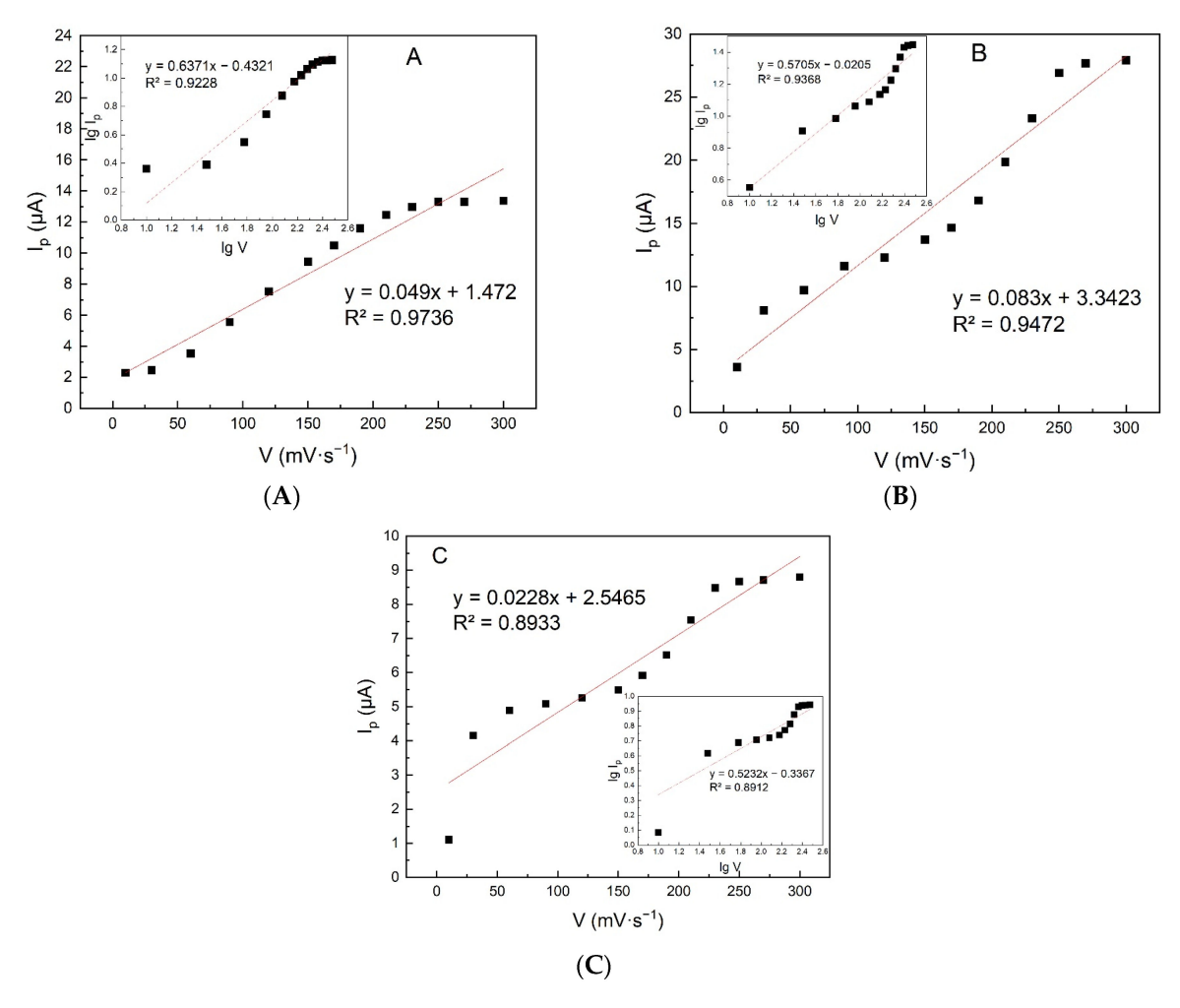


Figure 5. The dependence of LSV peak current of (A) NQ, (B) NQ1, (C) NQS on the scan rate v in $0.1 \text{ mol} \cdot L^{-1} \text{ NaClO}_4$ 96% ethanol solution at the IMGE vs. silver chloride electrode (1 mol·L⁻¹ KCl). Inset: Graph of lg I_p vs. lg v (Semerano criterion).

To study the oxidation–reduction mechanisms of naphthoquinones NQ, NQ1, and NQS, the dependence of the electro reduction current on $V^{1/2}$ was plotted (Figure 6) [48]. This dependence has a nonlinear character for all analyzed compounds. Moreover, the potential difference Δ Ep weakly depends on the potential scan rate. All the obtained data point to quasi-reversibility of the electrochemical process for NQ, NQ1 and NQS at the IMGE.

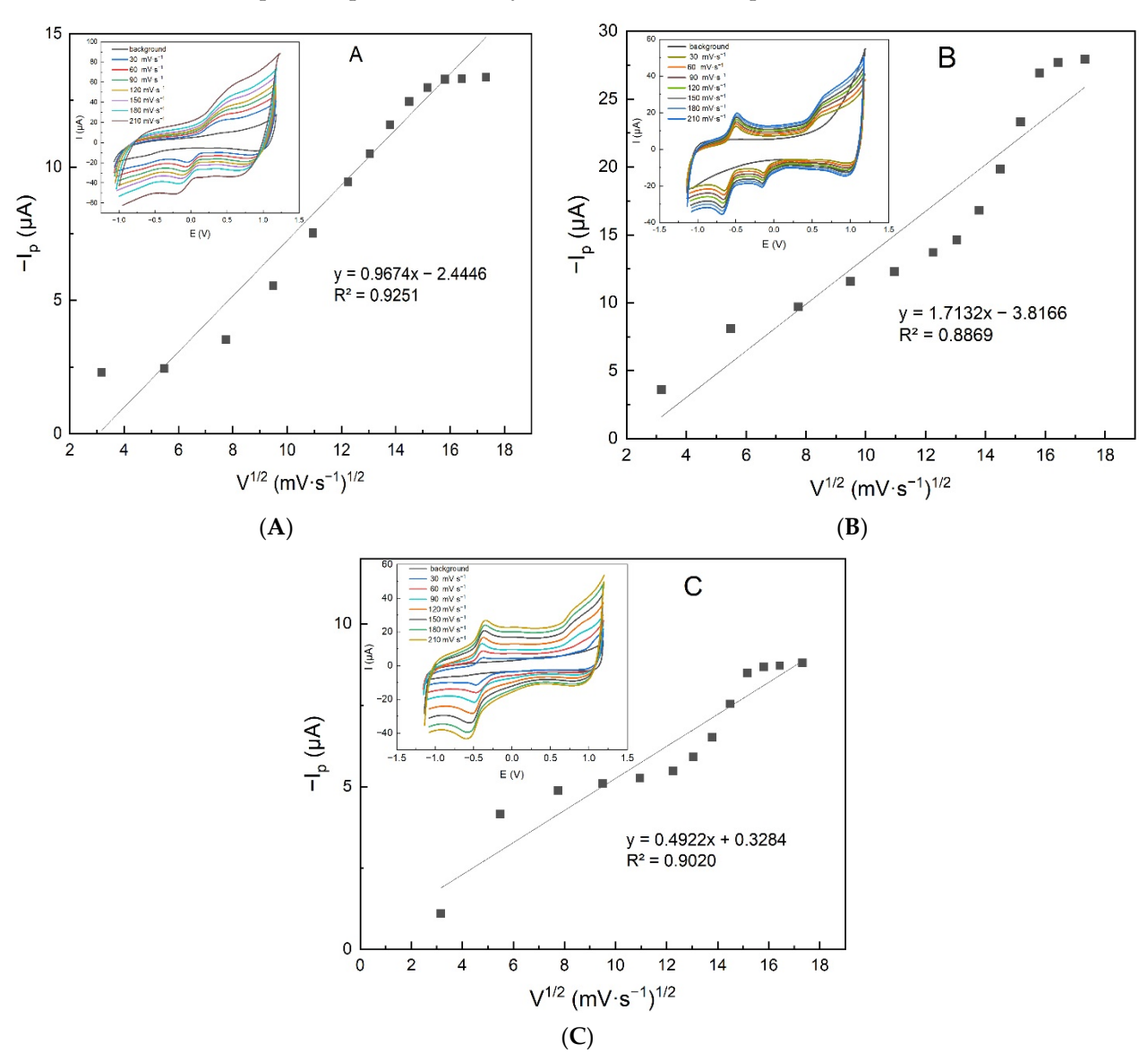


Figure 6. The dependence of the LSV reduction peak current on v1/2 in 0.1 M NaClO₄ 96% ethanol solution at the IMGE vs. silver chloride electrode (1 mol·L $^{-1}$ KCl). Inset: Cyclic voltammograms: NQ (A), NQ1 (B) and NQS (C) in 0.1 M NaClO₄ 96% ethanol solution (pH 4.0) at the IMGE vs. silver chloride electrode (1 mol·L $^{-1}$ KCl); v = 30–210 mV·s $^{-1}$.

It should be noted that we have not obtained any significant correlations between the electrochemical magnitudes and the DFT-derived characteristics (Table S2). Presumably, the electrode processes are to a great extent determined by adsorption of the compounds on the IMGE surface, which is not directly dependent on the electronic structure of the molecules.

2.3.2. Calculation of the Electron Number

The potential scan rate has great influence on the electrochemical process reversibility. As this rate increases, the process becomes more irreversible. Therefore, at low potential scan rates, it is possible to approximate a quasi-reversible process to a reversible one.

It is necessary to determine the relationship between the potentials of the anodic and cathodic peaks for an electrochemically reversible process to calculate the number of electrons involved in the electrochemical reaction (4) [48]:

$$\Delta Ep = 2.22 \times \frac{RT}{zF} = \frac{0.058}{z} \tag{4}$$

CV with a potential scan rate of $10 \text{ mv} \cdot \text{s}^{-1}$ was used for the experiment. The number of electrons involved in the electrochemical reaction corresponding to quinone (**NQ**) and imino (**NQ1**) groups was equal to 2, while for **NQS**, just one electron is transferred (imino group).

For all the investigated compounds, the following electrochemical mechanisms were proposed (Figure 7). The mechanism of **NQ** oxidation–reduction is in good agreement with the literature [49].

Figure 7. The proposed mechanism of electrochemical oxidation–reduction reactions (**A**) **NQ**, (**B**) **NQ1** and (**C**) **NQS** on the IMGE.

2.3.3. Voltammetric Determination of NQ, NQ1, and NQS by Linear Scan Voltammetry (LSV)

The experiment revealed the dependence of the **NQ** cathodic signal on pH of the background electrolyte (Figure 8A). HCl or NaOH was added to the background electrolyte to obtain the desired pH value. With the decrease in pH from 6 to 1, the **NQ** cathodic current increased significantly, with its maximum value reached at pH 2.0. With the increase in pH from 6 to 12, the cathodic current values of the **NQ** peak decreased significantly. This fact is explained by the participation of hydrogen ions in the electrochemical reaction, and the facilitation of electroreduction in acidic media [50].

It should be noted that accumulation parameters have a great influence on the analytical signals of the investigated compounds. As the accumulation potential increased, the **NQ** cathodic peak current also increased up to 1 V, followed by a slight decrease (Figure 8B); the accumulation time was 10 s. At the same time, when the accumulation was prolonged from 1 to 100 s at the selected accumulation potential of 1 V, the maximum of **NQ** cathodic peak current was observed at 50 s (Figure 8A).

At the same time, when the pH of the background electrolyte was increased from 2 to 12, the intensity of the **NQ1** anodic peak current and the **NQS** cathodic peak current grew significantly, with the maximum values being reached at pH 10.0 (Figure 9). This fact can be explained by a higher activity of the imino group in an alkaline medium [51,52].

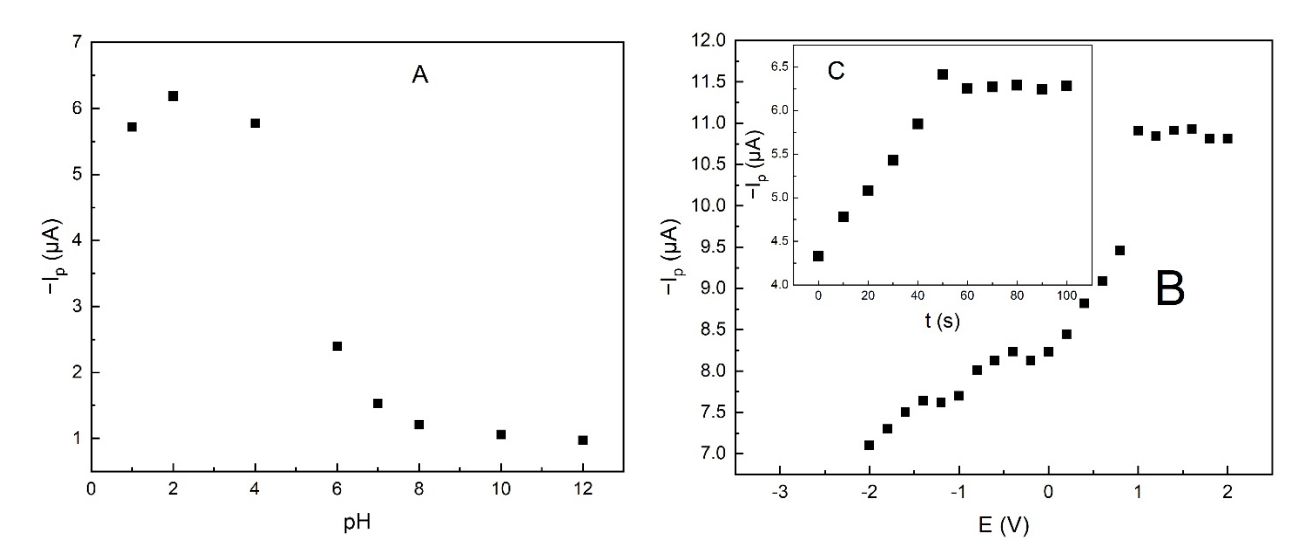


Figure 8. The dependence of **NQ** cathodic peak current measured by LSV on different parameters: (**A**) pH of the background electrolyte 0.1 M NaClO₄ 96% ethanol solution (without accumulation); (**B**) accumulation potential, V (pH 2.0; accumulation time 10 s); (**C**) accumulation time, s in 0.1 M NaClO₄ 96% ethanol solution (pH 2.0; accumulation potential 1 V) at the IMGE vs. silver chloride electrode (1 mol·L $^{-1}$ KCl); v = 100 mV·s $^{-1}$.

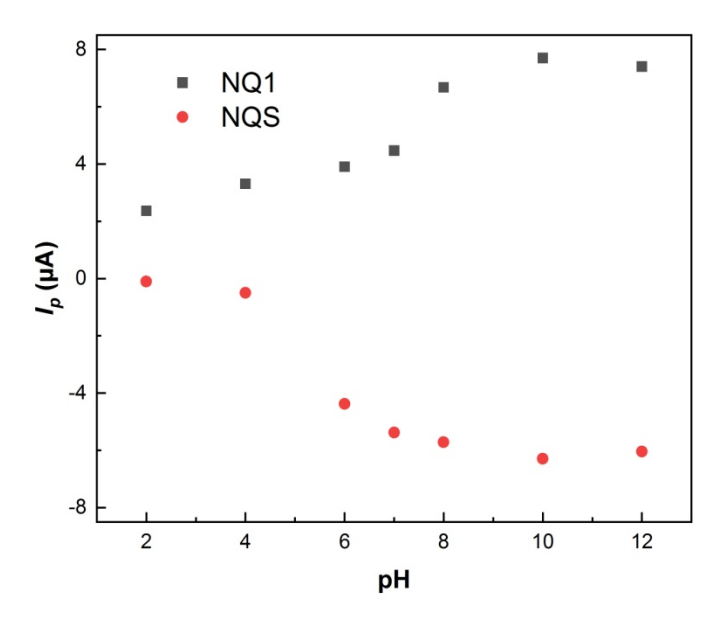


Figure 9. The dependence of the **NQ1** anodic peak current and **NQS** cathodic peak current measured by LSV on pH of the background electrolyte 0.1 M NaClO₄ 96% ethanol solution at the IMGE vs. silver chloride electrode (1 mol·L $^{-1}$ KCl); v = 100 mV·s $^{-1}$. HCl or NaOH was added to the background electrolyte to obtain the desired pH value.

The maximum values of the anodic (**NQ1**) and cathodic (**NQS**) peak currents were obtained at the accumulation potential of -1 V and -1.8 V, and accumulation time of 30 s and 20 s, respectively (Figure 10).

Optimal conditions for the voltammetric determination of **NQ**, **NQ1**, and **NQS** by linear scan voltammetry in the first derivative mode (LSVFD) at the IMGE are summarized in Table 6.

After selecting the optimal conditions for the LSVFD voltammetric determination of **NQ**, **NQ1** and **NQS**, the linear calibration plots of the analytical signal on the concentration of the investigated compounds in the model solutions were obtained using LSVFD (Figure 11 A–C).

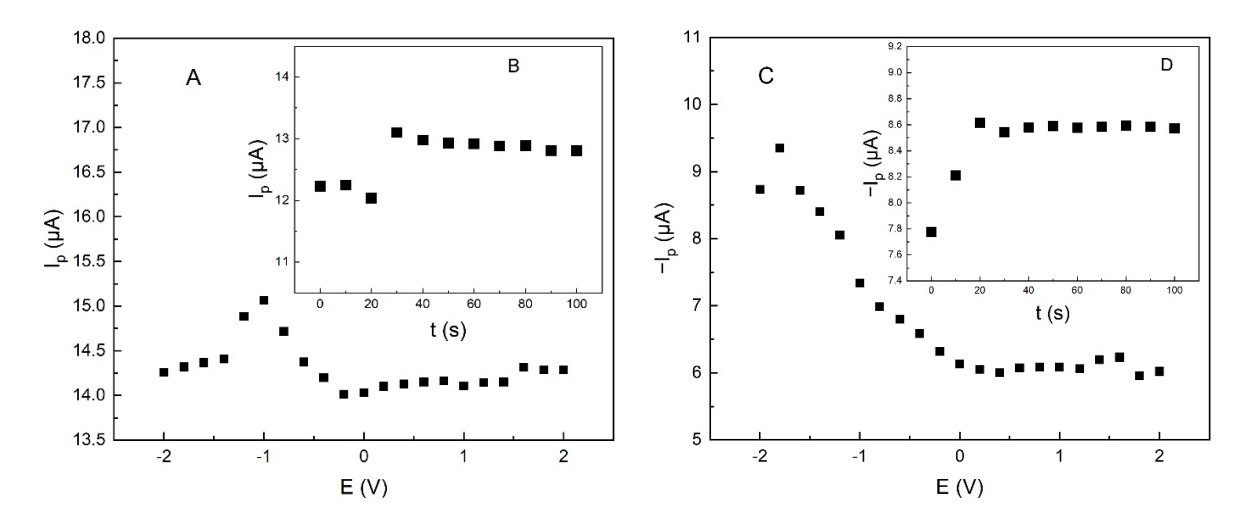


Figure 10. The dependence of NQ1 anodic peak current measured by LSV in 0.1 M NaClO₄ 96% ethanol solution on (A) accumulation potential, V (accumulation time 30 s); (B) accumulation time, s (accumulation potential -1.0 V) and NQS cathodic peak current measured by LSV in 0.1 M NaClO₄ 96% ethanol solution on (C) accumulation potential, V (accumulation time 20 s); (D) accumulation time, s (accumulation potential -1.8 V) at the IMGE vs. silver chloride electrode (1 mol·L⁻¹ KCl); v = 100 mV·s⁻¹.

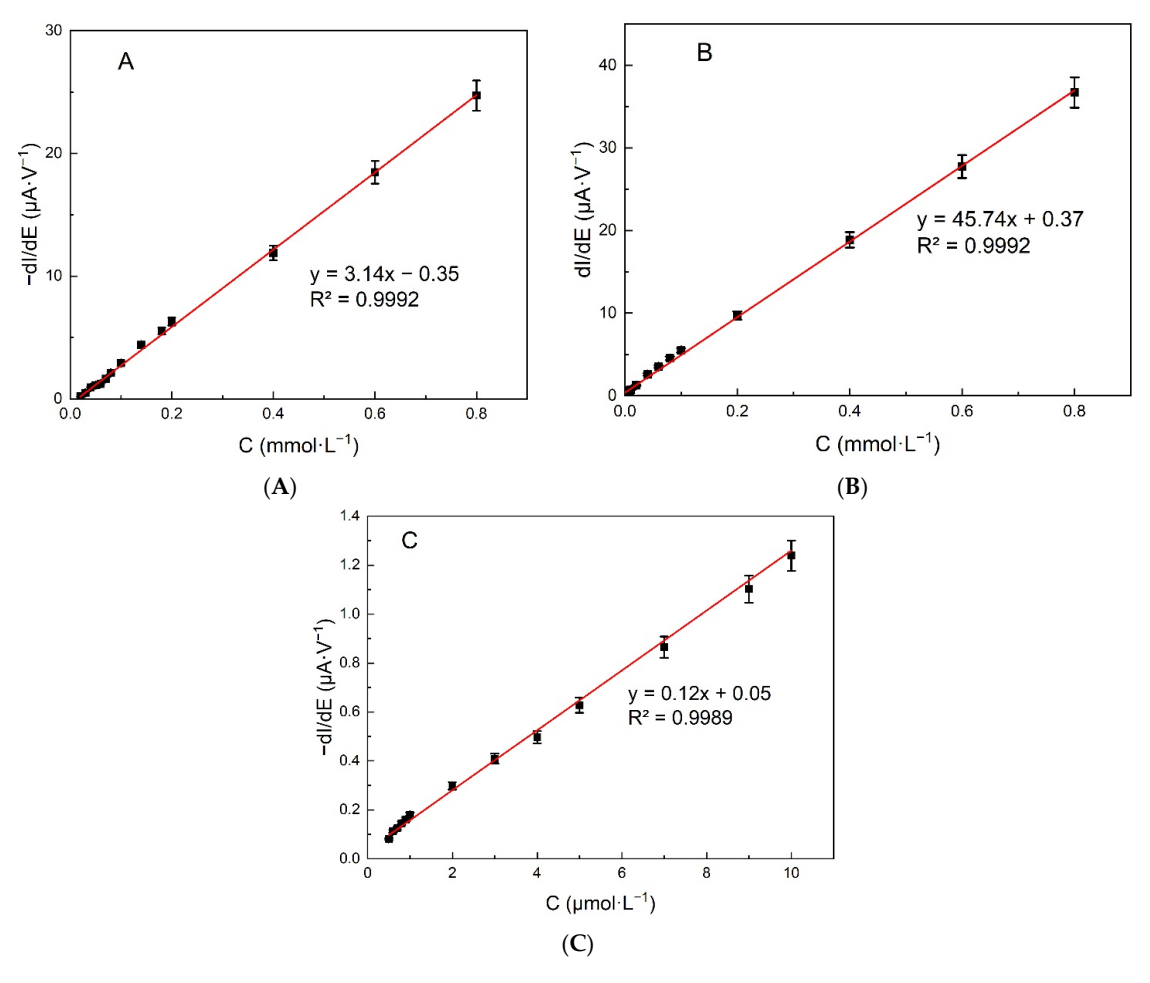


Figure 11. The linear plots of LSVFD peak current on the concentration of **(A)** NQ (pH 2.0) in the concentration range 2×10^{-5} –8 $\times 10^{-4}$ M; **(B)** NQ1 (pH 10.0) in the concentration range 1×10^{-6} –8 $\times 10^{-4}$ M; **(C)** NQS (pH 10.0) in the concentration range 5×10^{-7} –1 $\times 10^{-5}$ M in 0.1 M NaClO₄ 96% ethanol solution (pH 4.0) at the IMGE vs. silver chloride electrode (1 mol·L⁻¹ KCl); potential scan rate 100 mV·s⁻¹. The bars indicate standard deviations.

Parameter -	Optimal Conditions			
rarameter	NQ	NQ1	NQS	
Background electrolyte	0.1 M NaClO ₄ 96% ethanol solution			
Working electrode	IMGE			
Auxiliary/reference electrode	silver chloride electrode (1 mol· L^{-1} KCl)			
Scan rate, $mV \cdot s^{-1}$	100			
pН	2 10			
Accumulation potential, V	1.0	-1.0	-1.8	
Accumulation time, s	50	30	20	
Peak potential, V	0.13 ± 0.01	-0.58 ± 0.01	-0.52 ± 0.01	

Table 6. Optimal conditions for the LSVFD determination of NQ, NQ1, and NQS at the IMGE.

The pH values are indicated in the figure captions (Figure 11 A-C) and coincide with the data given in Table 6.

Parameters of the LSVFD determination of **NQ**, **NQ1**, and **NQS** in model solutions are summarized in Table 7.

Compound	Peak Potential, V	Regression Equation	Linear Concentration Range, mol·L $^{-1}$	Limit of Detection (LOD), $mol \cdot L^{-1}$
NQ	0.12	$y = 3.14x - 0.35$ $(R^2 = 0.9992)$	$2 \times 10^{-5} 8 \times 10^{-4}$	7.2×10^{-6}
NQ1	-0.58	$y = 45.74x + 0.37$ $(R^2 = 0.9992)$	$1 \times 10^{-6} - 8 \times 10^{-4}$	8×10^{-7}
NQS	-0.53	y = 0.12x + 0.05	5×10^{-7} – 1×10^{-5}	8.6×10^{-8}

Table 7. The parameters of LSVFD determination of **NQ**, **NQ1**, and **NQS** in model solutions (n = 5; p = 0.95).

2.3.4. Interference Study

The developed analytical technique can be used for the determination of newly synthesized 1,4-naphthoquinone derivatives in pharmaceutical preparations, which may contain some excipients. Therefore, it is necessary to determine the selectivity of the developed technique, namely to investigate the interfering effect of such compounds as sodium chloride, lactose, glucose, and sodium acetate.

The presence of interfering components in 10-fold excess reduces current intensity by a maximum of 13% (Figure 12A,B). Consequently, the obtained results show good selectivity in the determination of synthesized 1,4-naphthoquinone derivatives at the IMGE.

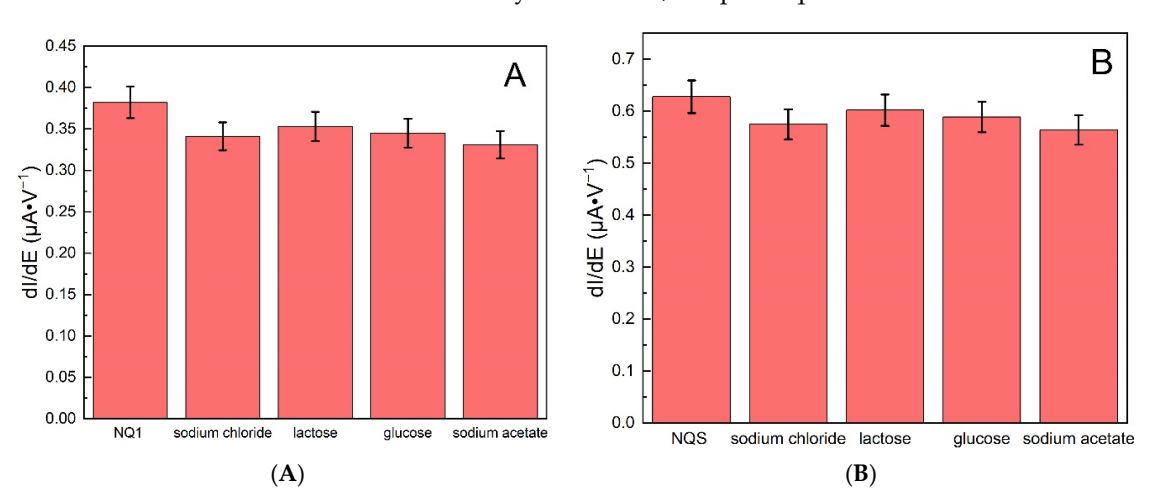


Figure 12. The influence of 10-fold excess of interfering components on the peak current of 5 μ mol·L⁻¹ solutions of (A) **NQ1** and (B) **NQS** at the IMGE obtained by LSVFD. Error bars indicate standard deviations.

Int. J. Mol. Sci. 2024, 25, 12245 17 of 25

2.3.5. Determination of NQ, NQ1, and NQS in Pharmaceutical Substances

The accuracy of the proposed methodology was determined by the "spiked test" method (Table 8).

Compound	Added ($mol \cdot L^{-1}$)	Found (mol· L^{-1})	Recovery (%)	Relative Standard Deviation (%)
	6×10^{-5}	6.06×10^{-5}	101	5.33
NQ	8×10^{-5}	7.95×10^{-5}	99.4	1.75
	1×10^{-4}	1.04×10^{-4}	104	3.74
	6×10^{-6}	6.04×10^{-6}	101	1.47
NQ1	8×10^{-6}	7.96×10^{-6}	99.5	1.5
	1×10^{-5}	0.97×10^{-5}	95	4.27
	6×10^{-7}	6.19×10^{-7}	103	3.94
NQS	1×10^{-6}	1.09×10^{-6}	109	9.06
	1.4×10^{-6}	$1.47\times\cdot10^{-6}$	105	18.33

Table 8. The LSVFD determination of NQ, NQ1 and NQS in pharmaceutical substances (n = 5; p = 0.95).

The results of LSVFD determination of NQ, NQ1, and NQS in pharmaceutical substances are satisfactory and indicate promising potential for future practical application.

3. Materials and Methods

3.1. Reagents and Equipment

All the reagents for synthesis were purchased from Sigma-Aldrich (St. Louis, Missouri, USA) or Acros Organics (Pittsburgh, PN, USA) and were used without further purification. LC/MS analysis was performed on an Agilent Infinity chromatograph (Santa Clara, CA, USA) with an Accurate Mass QTOF 6530 mass detector (Santa Clara, CA, USA). Chromatographic conditions: column Zorbax EclipsePlusC18 1.8 μ m, 2.1 \times 50 mm; eluent H_2O —acetonitrile (15:85%, v/v); flow rate 0.2 mL/min. Ionization source: ESI in positive mode. The ¹H, ¹³C, and ¹⁹F NMR spectra were recorded on a Bruker AVANCE III HD instrument (operating frequencies: ¹H—400 MHz; ¹³C—100 MHz; ¹⁹F—376 MHz). The spectra are presented in the Supplementary Materials (Figures S2-S11). Melting points of the obtained compounds were measured using a Melting Point Apparatus SMP30, heating rate 2.5 °C/min. The reaction mixture was monitored by thin layer chromatography (TLC) on Silufol UV-254 and Merck plates, silica gel 60, F254. Column chromatography was performed using Silica Gel 60 (0.040–0.063 mm).

Sodium hydroxide (NaOH), potassium chloride (KCl) and hydrochloric acid (HCl) for the electrochemical analysis were purchased from Sigma-Aldrich (St. Louis, Missouri, USA) and Sigma Tech (Khimki, Russia). A 0.1 M sodium perchlorate (NaClO₄) solution was prepared in 96% ethanol and used as the background electrolyte. HCl or NaOH was added to the background electrolyte to obtain the desired pH value. Deionized water was used to prepare all aqueous solutions for the electrochemical experiments. The stock solutions of the analyzed compounds with concentration $0.1 \text{ mol} \cdot L^{-1}$ were prepared in dimethylformamide. The solutions were stored for one month in amber bottles at room temperature.

3.2. Synthesis of Naphthoquinone Derivatives

3-Chloro-2-((4-hydroxyphenyl)amino)-1,4-naphthoquinone (NQ1) and 3-chloro-2-((3hydroxyphenyl)amino)-1,4-naphthoquinone (NQ2) were synthetized as described previously [53,54].

3.2.1. 3-Chloro-2-((4-(tert-butyldimethylsilyloxy)phenyl)amino)-1,4-naphthoquinone (NQ1a)

To a stirred solution of compound NQ1 (149.9 mg, 0.5 mmol) and imidazole (85.4 mg, 1.25 mmol) in dichloromethane (DCM, 3 mL), a TBSCl solution (113 mg, 0.75 mmol) in DCM (0.5 mL) was added dropwise at 0 °C. The reaction mixture was stirred for 4 h at room temperature, extracted twice with 10 mL DCM, and washed with brine. The organic

layer was dried with anhydrous Na₂SO₄, filtered, and evaporated in vacuo. The residue was crystallized from ethanol. Yield 99%. M.p. 191–192 °C. ¹H NMR (CDCl₃), δ , ppm: 8.18 (1H, d, J = 8 Hz, H-4), 8.10 (1H, d, J = 8 Hz, H-1), 7.76 (1H, td, J = 8 Hz, 1.3 Hz, H-3), 7.67 (1H, td, J = 8 Hz, 1.3 Hz, H-2), 7.64 (1H, s, NH), 6.99 (2H, d, J = 8 Hz, H-6, H-7), 6.81 (2H, d, J = 8 Hz, H-5, H-8), 0.99 (9H, s, t-Bu), 0.21 (6H, s, SCH₃). The atom numbering used for the ¹H NMR signal assignments are shown in Figure 13. ¹³C NMR (CDCl₃), δ , ppm: 180.6, 177.5, 154.0, 141.9, 135.0, 132.8, 132.7, 130.9, 129.8, 127.1, 126.9, 126.3, 119.9, 113.5, 25.7, 18.3, -4.4. Found, %: C, 63.55; H, 5.72; N, 3.51; C₂₂H₂₄ClNO₃Si. Calculated, %: C, 63.83; H, 5.84; N, 3.38.

Figure 13. The atom numbering used for signal assignments in the ¹H NMR spectra.

3.2.2. 3-Chloro-2-((3-(tert-butyldimethylsilyloxy)phenyl)amino)-1,4-naphthoquinone (NQ2a)

The synthesis of **NQ2a** was carried out as described above for obtaining compound **NQ1a**, using **NQ2** as a starting material. Yield 96%. M.p. 188–189 °C. ¹H NMR (CDCl₃), δ , ppm: 8.19 (1H, d, J = 8 Hz, H-4), 8.11 (1H, d, J = 8 Hz, H-1), 7.77 (1H, t, J = 8 Hz, H-3), 7.69 (1H, t, J = 8 Hz, H-2), 7.63 (1H, s, NH), 7.18 (1H, t, J = 8 Hz, H-7), 6.70 (2H, d, J = 8 Hz, H-6, H-8), 6.57 (1H, s, H-5), 0.98 (9H, s, t-Bu), 0.21 (6H, s, SCH₃). ¹³C NMR (DMSO-d₆), δ , ppm: 180.5, 177.2, 155.3, 143.7, 140.5, 135.2, 133.7, 132.4, 130.8, 129.1, 127.0, 126.6, 117.8, 116.5, 116.0, 115.1, 26.0, 18.4, -4.0. Found, %: C, 63.76; H, 5.68; N, 3.49; C₂₂H₂₄ClNO₃Si. Calculated, %: C, 63.83; H, 5.84; N, 3.38.

3.2.3. 4-((3-Chloro-1,4-naphthoquinon-2-yl)amino)phenyl fluorosulfate (NQS)

Chamber A of a two-chamber reactor (Figure S1) was filled with 1,1'-sulfonyldiimidazole (SDI, 495 mg, 2.5 mmol) and potassium fluoride (378 mg, 6.5 mmol). Next, chamber B was charged with compound NQ1a (207 mg, 0.5 mmol), DBU (75 μL, 0.5 mmol), and DCM (3 mL). Finally, 1.6 mL formic acid was added by injection through the septum in the cap of chamber A, and instant gas formation was observed. After 24 h stirring at room temperature, one of the caps was carefully opened to release the residual pressure. The reaction mixture was stirred for another 15 min to ensure that all sulfuryl fluoride was removed. Next, the content of chamber B was transferred to a 100 mL round-bottomed flask. Chamber B was rinsed two times with 2 mL of DCM, and these fractions were added to the same flask. Then, the solvent was removed under reduced pressure. The crude product was purified by column chromatography on silica gel (eluent chloroform). Compound **NQS** was obtained as orange crystals. Yield 95%. M.p. 213–214 °C. ¹H NMR (DMSO-d₆), δ, ppm: 9.46 (1H, s, NH), 8.04 (2H, d, *J* = 8 Hz, H-1, H-4), 7.87 (1H, td, *J* = 7, Hz 1.2 Hz, H-3(2)), 7.82 (1H, td, J = 7 Hz, 1.2 Hz, H-2(3)), 7.53 (2H, d, J = 9 Hz, H-6, H-7), 7.28 (2H, d, J = 9 Hz, H-7), 7.28 (2H, d, JH-5, H-8). ¹³C NMR (DMSO-d₆), δ, ppm: 180.4, 177.4, 145.9, 143.5, 140.3, 135.2, 133.9, 132.3, 130.9, 127.1, 126.6, 125.3, 121.2, 117.0. ¹⁹F NMR (DMSO-d₆), δ, ppm: 38.34. LC/MS (ESI+); m/z: 381.9945 [M + H]⁺ experimental ([C₁₆H₉ClFNO₅S + H]⁺ = 381.9947 theor.).

The yield of **NQS** was 8% when using compound **NQ1** as a starting material.

3.2.4. 3-((3-Chloro-1,4-naphthoquinon-2-yl)amino)phenyl fluorosulfate (NQS2)

The synthesis of **NQS2** was carried out as described above for obtaining compound **NQS**, using compound **NQ2a** as a starting material. Yield 85%. M.p. 198–200 °C. ¹H NMR (DMSO-d₆), δ , ppm: 9.52 (1H, s, NH), 8.05 (2H, d, J = 8 Hz, H-1, H-4), 7.88 (1H, td, J = 7 Hz, 1.2 Hz, H-3(2)) 7.83 (1H, td, J = 7 Hz, 1.2 Hz, H-2(3)), 7.50 (1H, t, J = 8 Hz, H-7), 7.33

(1H, s, H-5), 7.25–7.30 (2H, m, H-6, H-8),. 13 C NMR (DMSO-d₆), δ , ppm: 180.4, 177.5, 149.6, 143.3, 141.9, 135.2, 133.9, 132.2, 130.9, 130.4, 127.0, 126.6, 123.7, 118.0, 116.2, 115.8. 19 F NMR (DMSO-d₆), δ , ppm: 38.84. LC/MS (ESI+); m/z: 381.9947 [M + H]⁺ experimental ([C₁₆H₉CIFNO₅S + H]⁺ = 381.9947 theor.).

The yield of **NQS2** was 9% when using compound **NQ2** as a starting material.

3.2.5. Method of One-Pot Synthesis 4-((3-Chloro-1,4-naphthoquinon-2-yl)amino)phenyl fluorosulfate (NQS) and 3-((3-Chloro-1,4-naphthoquinon-2-yl)amino)phenyl fluorosulfate (NQS2)

Chamber A of a two-chamber reactor (Figure S1) was filled with 1,1'-sulfonyldiimidazole (SDI, 495 mg, 2.5 mmol) and potassium fluoride (378 mg, 6.5 mmol). Next, chamber B was charged with compound NQ1 (149.9 mg, 0.5 mmol), imidazole (85.4 mg, 1.25 mmol) in dichloromethane (DCM, 3 mL), and a TBSCl solution (113 mg, 0.75 mmol) in DCM (0.5 mL) was added dropwise at 0 °C. The reaction mixture in chamber B was stirred for 4 h at room temperature (the presence of **NQ1** was controlled by TLC in CHCl₃). After finishing reaction, a DBU (75 µL, 0.5 mmol) was added in chamber B, and both reactor caps were tightly closed. Finally, 1.6 mL formic acid was added by injection through the septum in the cap of chamber A, and instant gas formation was observed. After 24 h stirring at room temperature, one of the caps was carefully opened to release the residual pressure. The reaction mixture was stirred for another 15 min to ensure that all sulfuryl fluoride was removed. Next, the content of chamber B was transferred to a 100 mL round-bottom flask. Chamber B was rinsed two times with 2 mL of DCM, and these fractions were added to the same flask. Then, the solvent was removed under reduced pressure. The crude product NQS was purified by column chromatography on silica gel (eluent chloroform). Yield 32%. Spectra as described above.

The synthesis of **NQS2** was carried out the same way using compound **NQ2** as a starting material. Yield 22%. Spectra as described above.

3.3. Biological Experiments

Cell line preparation. PC-3 (prostatic adenocarcinoma), SKOV-3 (ovarian cancer), MCF-7 (breast cancer) cell lines (PrimeBioMed LLC, Moscow, Russia) were grown in Dulbecco's modified eagle medium (DMEM, Gibco, Billings, MT, USA). Cultivation was carried out under standard conditions in a CO₂-incubator CB-170 (Binder, Germany) with 5% CO₂ at 37 °C and 100% humidity. The cells were thus brought into the stable growth phase and were used for the experiments.

Cell viability tests. To evaluate the cytotoxic effects, 5000 cells (counted by automated cell counter Countess 2FL (Thermo Fisher Scientific Inc., Waltham, MA, USA) per well were seeded into wells of a 96-well sterile plate (SPL Life Sciences Co., Naechon-myeon, Republic of Korea) at 24 h before the start of the tests. The cells adhered and adapted to the substrate during this period. Following this, the medium was replaced with fresh medium containing serial dilutions of the test compounds to evaluate their effects. Media contained 50 μ M, 25 μ M, 12.5 μ M, 6.25 μ M, 3.13 μ M, 1.56 μ M, 0.78 μ M, 0.39 μ M concentration for each tested compound. All plates were placed in an incubator and cultured under standard conditions at 37 °C and 5% CO₂.

To assess cell viability, MTT assays were employed after a 24-h incubation period. Specifically, the DMEM medium in the wells was replaced with a 0.45 mg/mL solution of 3-(4,5-dimethylthiazol-2-yl)-2,5-diphenyl-2H-tetrazolium bromide (MTT, PanEco Ltd., Moscow, Russia). The plate was then incubated in a CO₂-incubator at 37 °C for 4 h. Following incubation, the MTT solution was aspirated, and 100 μ L of dimethyl sulfoxide (DMSO, PanEco Ltd., Moscow, Russia) was added to solubilize the formazan crystals. The optical density of the resulting solution was measured at 570 nm using a Multiskan FC microplate photometer (Thermo Fisher Scientific Inc., Waltham, MA, USA). Data were analyzed, and cell viability was expressed as a percentage relative to the control group. An extended viability assessment was conducted using the Jurkat cell line. For this, 40,000 cells per well, counted via the automated cell counter Countess 2FL (Thermo Fisher Scientific

Inc., Waltham, MA, USA), were seeded into a sterile 96-well plate (SPL Life Sciences Co., Naechon-myeon, Republic of Korea). All compounds were added in serial dilutions at identical concentrations. After 24 h of incubation, cytofluorimetric measurement (CytoFlex, Beckman Coulter, Brea, CA, USA) of cell death variants, cell viability and the level of reactive oxygen species (ROS) production was performed with Annexin V-FITC Apoptosis Detection Kit (Abcam, Cambridge, UK and Cellular ROS Assay Kit (Abcam, UK) according to manufacturer's protocol. All the tests were performed in 6 replications.

3.4. DFT Calculations

The structures of the studied naphthoquinones were constructed and preliminarily optimized using the semi-empirical PM3 method with the HyperChem 7 software (Hypercube, Inc., Gainesville, FL, USA). DFT calculations were performed using the ORCA 4.2 program (Max Planck Institute for Coal Research, Mülheim/Ruhr, Germany, December 2018) on a computer running Windows Server 2016 (CPU 16×2.4 GHz, 16 GB RAM). The BP86 functional [55], the def2-TZVPP basis set [56], the RI approximation with the auxiliary basis set def2/J [57], and the D3BJ dispersion correction [58] were used. The attainment of real energy minima during geometry optimization in the gas phase was confirmed by calculating the frequencies of normal vibrations. Subsequently, for the energy minimum found for each compound, a single point energy calculation was performed without geometry optimization using the ω B97X-D3 functional [45] and the 6_311++G(3df,3pd) basis set with the RIJCOSX approximation [59,60], along with auxiliary basis sets generated by the AutoAux procedure [57]. To evaluate the vertical electron affinity (VEA), "single point" energies of anion radicals were calculated, whose geometries corresponded to the optimized structures of the respective neutral naphthoquinones. The ωB97X-D3 functional were used for these calculations, as described above. The obtained results were visualized and analyzed using the Chemcraft program (https://www.chemcraftprog.com, accessed on 20 June 2024).

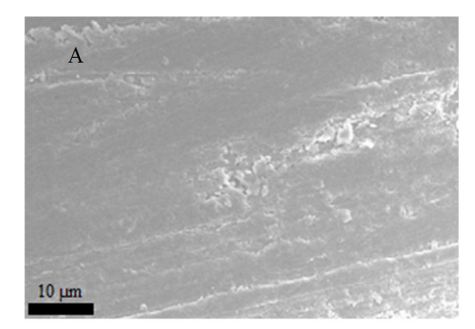
3.5. Electrochemical Measurements

3.5.1. Equipment

Cyclic voltammetry (CV) and linear scan voltammetry in the first derivative mode (LSVFD) were performed with TA-Lab voltammetric analyzer in a conventional three-electrode cell (Tomanalyt, Tomsk, Russia). IMGE was used as a working electrode, silver/silver chloride electrodes (1 $\text{mol} \cdot \text{L}^{-1}$ KCl) were used as counter and reference electrodes. The analyzer Itan (pH-meter/ionomer) was used for pH measurement. All the experiments were carried out at room temperature. The surface of the IMGE was examined using a JEOL JSM-7500FA scanning electron microscope (SEM) operated at an accelerating voltage of 10 kV and equipped with a field emission cathode and a secondary electron (SE) detector.

3.5.2. Characterization of the IMGE

IMGE represents a disk graphite electrode impregnated with polyethylene and paraffin under vacuum [61]. The general SEM image obtained for the electrode surface is shown in Figure 14A.



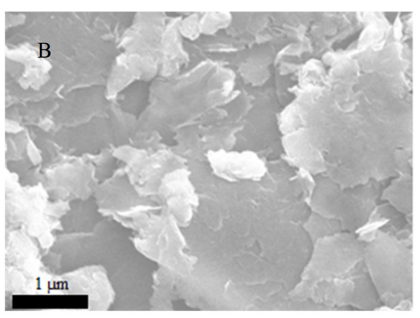


Figure 14. SEM images of the IMGE in SE mode: (A) at 1000 magnification; (B) at 10000 magnification.

The electrode material is composite. This means that it retains micro porosity due to the nonregular distribution of polyethylene and paraffin (phase) during the impregnation procedure. Figure 14B shows traces of impregnate (a mixture of polyethylene and paraffin), as well as scratches arising from mechanical cleaning of the IMGE surface on the ashless filter. Moreover, residual pores from the primary graphite blank also appear on the surface of the IMGE.

The presence of micropores with a diameter of about 2 μm surrounded by individual pores with a smaller diameter of about 200 nm is observed under sufficient magnification (Figure 14B). Consequently, it is possible to assume that an adsorption process on the electrode surface plays a sufficient role during electrochemical measurements.

The redox pair $[Fe(CN)_6]^{3-}$ / $[Fe(CN)_6]^{4-}$ is widely used for evaluation of the IMGE efficiency as a working electrode. Figure 15 shows cyclic voltammograms of $[Fe(CN)_6]^{3-}$ / $[Fe(CN)_6]^{4-}$ at the IMGE. CV was used to calculate the value of the IMGE electroactive surface area, namely, the redox current of $[Fe(CN)_6]^{3-}$ / $[Fe(CN)_6]^{4-}$ was recorded with the potential scan rate from 20 to 200 mV·s⁻¹.

The value of electroactive surface area of IMGE was estimated as 0.059 cm² using the Randles–Ševčík equation [62].

Electrochemical properties of the electrode were also evaluated through impedance spectroscopy (EIS). Figure 16A shows the EIS spectra of the IMGE in the capacity coordinates in the phosphate buffer solution (PBS), pH 6.86. The resulting spectrum corresponds to an equivalent electrical circuit (Figure 16A inset). The accuracy of the selected scheme is confirmed by the small error values of the simulated circuit elements, less than 5% and by the value of the criterion $\chi^2 = 5.7 \times 10^{-3}$. Double layer capacitance (C_{dl}) value was calculated as 2.148 µF [63].

Only solvated ions, which are responsible for the presence of the double layer capacitance, are present in PBS. When the $[Fe(CN)_6]^{3-}/[Fe(CN)_6]^{4-}$ probe is applied, a component appears that passes through the double layer and can diffuse near the electrode surface. The impedance spectrum of the IMGE in a solution of $5\cdot10^{-3}$ mol·L⁻¹ $[Fe(CN)_6]^{3-}/[Fe(CN)_6]^{4-}$ in 0.1 mol·L⁻¹ KCl in Nyquist coordinates is shown in Figure 16B. The resulting spectrum corresponds to an equivalent electrical circuit (Figure 16B inset). The value of the criterion $\chi^2=4\times10^{-4}$; the R_{ct} value is 6.94 k Ω and is acceptable for measurements at IMGE.

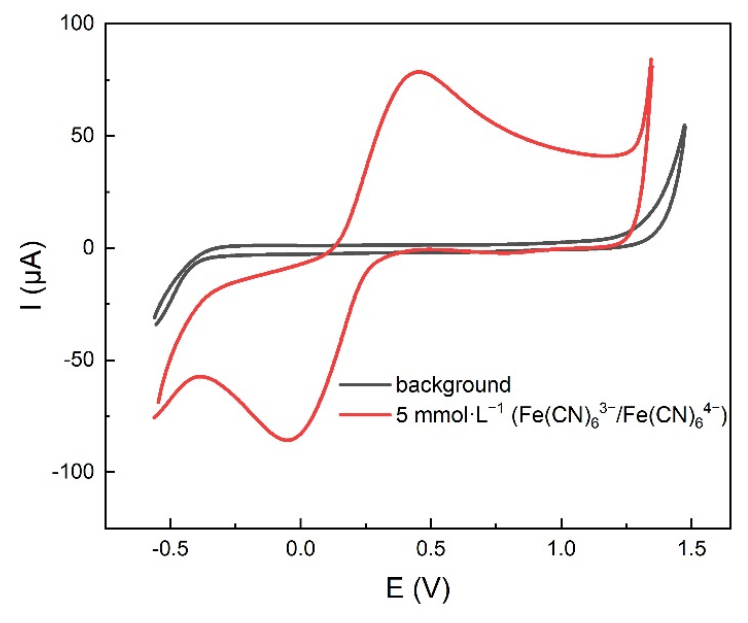


Figure 15. Cyclic voltammograms of $5 \cdot 10^{-3} \text{ mol} \cdot L^{-1}$ [Fe(CN)₆]³⁻/[Fe(CN)₆]⁴⁻ in 1 mol·L⁻¹ KCl at the IMGE, v =100 mV·s⁻¹.

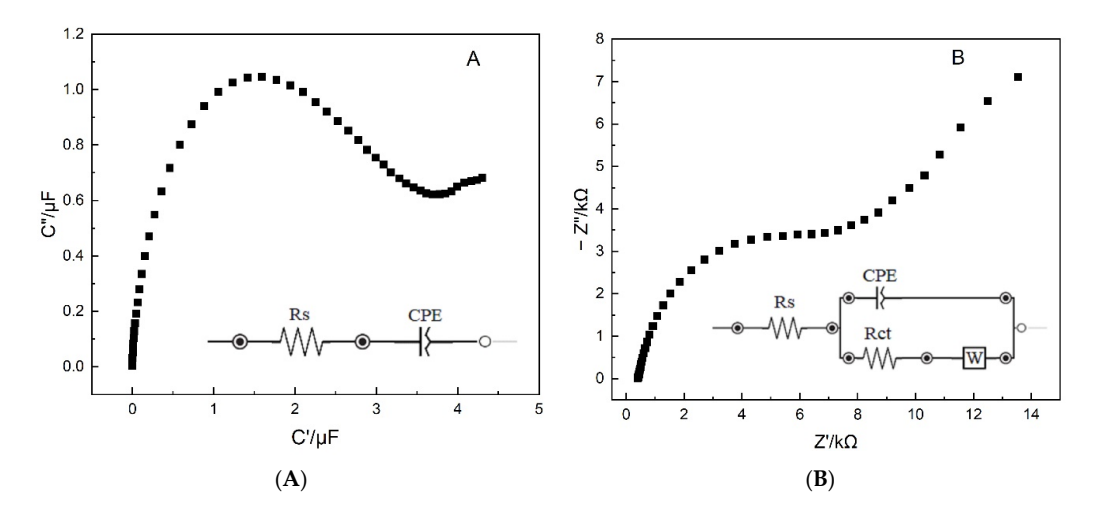


Figure 16. The EIS spectra of the IMGE (**A**) in the capacity coordinates in PBS solution (pH 6.86); (**B**) in the presence of $5\cdot10^{-3}$ mol·L⁻¹ [Fe(CN)₆]³⁻/[Fe(CN)₆]⁴⁻ in 0.1 mol·L⁻¹ KCl in Nyquist coordinates. Inset: equivalent electrical circuits (Rs—solution resistance; CPE—constant phase element (replaces the capacitance); Rct—the charge transfer resistance; W—Warburg element).

The obtained values of the double layer capacitance and charge transfer resistance indicate that the oxidation and reduction processes at the IMGE occur without any difficulties. Therefore, it can be anticipated that other compounds will be easily oxidized and reduced on this surface.

3.6. ADME Predictions

The ADME and physicochemical properties of selected compounds were computed using SwissADME (http://www.swissadme.ch, accessed on 2 September 2024).

4. Conclusions

This work reported for the first time the preparation of fluorosulfate derivatives of naphthoquinone. It was shown that these compounds had cytotoxic activities against PC-3 (prostatic adenocarcinoma), SKOV-3 (ovarian cancer), MCF-7 (breast cancer) cell lines and possess satisfactory bioavailability and toxicity parameters. The parameters of apoptosis, cell viability and the level of production of reactive oxygen species (ROS) were studied on the Jurkat cell line. A voltammetric technique for the determination of 1,4-naphthoquinone derivatives at the IMGE was developed. As a result of the studies conducted with the use of IMGE, we established the nature of the oxidation–reduction processes of the analyzed compounds NQ, NQ1, and NQS. Namely, for all the analytes, the process was characterized as quasi-reversible with the participation of two electrons for NQ and NQ1 and one electron for NQS.

The LSVFD was used to obtain the calibration curves of the analytical signal vs. concentration of the investigated compounds under the optimal experimental conditions with LOD $7.2 \times 10^{-6} \text{ mol} \cdot \text{L}^{-1}$ for NQ, $8 \times 10^{-7} \text{ mol} \cdot \text{L}^{-1}$ for NQ1, and $8.6 \times 10^{-8} \text{ mol} \cdot \text{L}^{-1}$ for NOS.

The proposed technique was successfully applied for the determination of compounds in the substance by the spiked-test method. The use of IMGE provides a promising opportunity not only to investigate the nature of electrochemical reactions of 1,4-naphthoquinones, but also to use a simple and rapid technique for the determination of the naphthoquinone derivatives both in pharmaceutical substances and in real objects.

Supplementary Materials: The following supporting information can be downloaded at: https://www.mdpi.com/article/10.3390/ijms252212245/s1. Figure S1: the two-chamber reactor; Figures S2–S11: the NMR spectra; Table S1: PASS prediction of biological activities for the naphthoquinone derivatives; Table S2: results of the DFT calculations.

Author Contributions: N.V.D., N.V.A. and A.I.K.: conceptualization; N.V.D., N.V.A., E.V.P., E.I.K., A.V.E., D.D.E. and A.N.S.: methodology and experimental work; N.V.A., N.V.D., E.V.P., O.I.L. and A.I.K.: data analysis, writing, and editing the manuscript; A.I.K. and E.I.K.: project administration and supervision; A.I.K.: funding acquisition. All authors have read and agreed to the published version of the manuscript.

Funding: The synthesis of naphthoquinone derivatives, the molecular modeling and biological activity studies were supported by the Russian Science Foundation (project No. 24-15-00334).

Institutional Review Board Statement: Not applicable.

Informed Consent Statement: Not applicable.

Data Availability Statement: The data presented in this study are available in this article.

Acknowledgments: The authors acknowledge the support from the Tomsk Polytechnic University development program for conducting the electrochemistry experiments.

Conflicts of Interest: The authors declare no conflicts of interest.

References

 Uchimiya, M.; Stone, A.T. Reversible Redox Chemistry of Quinones: Impact on Biogeochemical Cycles. Chemosphere 2009, 77, 451–458. [CrossRef] [PubMed]

- 2. Halicki, P.C.B.; Ferreira, L.A.; De Moura, K.C.G.; Carneiro, P.F.; Del Rio, K.P.; Carvalho, T.d.S.C.; Pinto, M.d.C.F.R.; da Silva, P.E.A.; Ramos, D.F. Naphthoquinone Derivatives as Scaffold to Develop New Drugs for Tuberculosis Treatment. *Front. Microbiol.* **2018**, *9*, 673. [CrossRef] [PubMed]
- 3. Patel, O.P.S.; Beteck, R.M.; Legoabe, L.J. Antimalarial Application of Quinones: A Recent Update. *Eur. J. Med. Chem.* **2021**, 210, 113084. [CrossRef] [PubMed]
- 4. Leote, R.J.B.; Sanz, C.G.; Diculescu, V.C. Electrochemical Characterization of Shikonin and In-Situ Evaluation of Interaction with DNA. *J. Electroanal. Chem.* **2022**, 921, 116663. [CrossRef]
- 5. Lebedev, A.V.; Ivanova, M.V.; Levitsky, D.O. Iron Chelators and Free Radical Scavengers in Naturally Occurring Polyhydroxylated 1,4-Naphthoquinones. *Hemoglobin* **2008**, 32, 165–179. [CrossRef]
- 6. Devine, A.; Hegarty, C.; Casimero, C.; Molyneaux, R.L.; Smith, R.B.; Cardosi, M.F.; Davis, J. Electrochemically Initiated Release: Exploring New Modalities for Controlled Drug Release. *J. Electroanal. Chem.* **2020**, *872*, 113926. [CrossRef]
- 7. Krayz, G.T.; Bittner, S.; Dhiman, A.; Becker, J.Y. Electrochemistry of Quinones with Respect to Their Role in Biomedical Chemistry. *Chem. Rec.* **2021**, *21*, 2332–2343. [CrossRef]
- 8. Rahman, M.M.; Islam, M.R.; Akash, S.; Shohag, S.; Ahmed, L.; Supti, F.A.; Rauf, A.; Aljohani, A.S.M.; Al Abdulmonem, W.; Khalil, A.A.; et al. Naphthoquinones and Derivatives as Potential Anticancer Agents: An Updated Review. *Chem. Biol. Interact.* **2022**, 368, 110198. [CrossRef]
- 9. Newman, D.K.; Kolter, R. A Role for Excreted Quinones in Extracellular Electron Transfer. Nature 2000, 405, 94–97. [CrossRef]
- 10. Turek, A.K.; Hardee, D.J.; Ullman, A.M.; Nocera, D.G.; Jacobsen, E.N. Activation of Electron-Deficient Quinones through Hydrogen-Bond-Donor-Coupled Electron Transfer. *Angew. Chemie Int. Ed.* **2016**, *55*, 539–544. [CrossRef]
- 11. Ibis, C.; Shntaif, H.; Bahar, H.; Ayla, S. An Investigation of Nucleophilic Substitution Reactions of 2,3-Dichloro-1,4-Naphthoquinone with Various Nucleophilic Reagents. *J. Serbian Chem. Soc.* **2015**, *80*, 731–738. [CrossRef]
- 12. Kacmaz, A.; Acar, E.T.; Atun, G.; Kaya, K.; Sigirci, B.D.; Bagcigil, F. Synthesis, Electrochemistry, DFT Calculations, Antimicrobial Properties and X-ray Crystal Structures of Some NH- and/or S-Substituted-1,4-quinones. *ChemistrySelect* 2018, 3, 8615–8623. [CrossRef]
- 13. Ravichandiran, P.; Masłyk, M.; Sheet, S.; Janeczko, M.; Premnath, D.; Kim, A.R.; Park, B.; Han, M.; Yoo, D.J. Synthesis and Antimicrobial Evaluation of 1,4-Naphthoquinone Derivatives as Potential Antibacterial Agents. *ChemistryOpen* **2019**, *8*, 589–600. [CrossRef] [PubMed]
- 14. Tandon, V.K.; Yadav, D.B.; Singh, R.V.; Vaish, M.; Chaturvedi, A.K.; Shukla, P.K. Synthesis and Biological Evaluation of Novel 1,4-Naphthoquinone Derivatives as Antibacterial and Antiviral Agents. *Bioorg. Med. Chem. Lett.* **2005**, *15*, 3463–3466. [CrossRef] [PubMed]
- 15. Kim, B.H.; Yoo, J.; Park, S.-H.; Jung, J.-K.; Cho, H.; Chung, Y. Synthesis and Evaluation of Antitumor Activity of Novel 1,4-Naphthoquinone Derivatives (IV). *Arch. Pharm. Res.* **2006**, 29, 123–130. [CrossRef]
- 16. Kacmaz, A.; Deniz, N.G.; Aydinli, S.G.; Sayil, C.; Onay-Ucar, E.; Mertoglu, E.; Arda, N. Synthesis and Antiproliferative Evaluation of Some 1,4-Naphthoquinone Derivatives against Human Cervical Cancer Cells. *Open Chem.* **2019**, 17, 337–345. [CrossRef]
- 17. Schepetkin, I.A.; Karpenko, A.S.; Khlebnikov, A.I.; Shibinska, M.O.; Levandovskiy, I.A.; Kirpotina, L.N.; Danilenko, N.V.; Quinn, M.T. Synthesis, Anticancer Activity, and Molecular Modeling of 1,4-Naphthoquinones That Inhibit MKK7 and Cdc25. *Eur. J. Med. Chem.* 2019, 183, 111719. [CrossRef]
- 18. Wellington, K.W. Understanding Cancer and the Anticancer Activities of Naphthoquinones—A Review. *RSC Adv.* **2015**, 5, 20309–20338. [CrossRef]
- 19. Dong, J.; Krasnova, L.; Finn, M.G.; Sharpless, K.B. Sulfur(VI) Fluoride Exchange (SuFEx): Another Good Reaction for Click Chemistry. *Angew. Chemie Int. Ed.* **2014**, *53*, 9430–9448. [CrossRef]

20. Liu, Z.; Li, J.; Li, S.; Li, G.; Sharpless, K.B.; Wu, P. SuFEx Click Chemistry Enabled Late-Stage Drug Functionalization. *J. Am. Chem. Soc.* 2018, 140, 2919–2925. [CrossRef]

- 21. Chai, J.; Zhang, J.; Wen, Y.; Zou, L.; Zhang, X.; Xin, X.; Zhou, M.; Xu, J.; Zhang, G. Highly Sensitive Electrochemical Sensor Based on PEDOT:PSS-β-CD-SWCNT-COOH Modified Glassy Carbon Electrode Enables Trace Analysis Shikonin. *J. Electrochem. Soc.* **2019**, *166*, B388–B394. [CrossRef]
- 22. Wu, L.; Lu, L.; Zhang, L.; Xu, J.; Zhang, K.; Wen, Y.; Duan, X.; Yang, F. Electrochemical Determination of the Anticancer Herbal Drug Shikonin at a Nanostructured Poly(Hydroxymethylated-3,4-ethylenedioxythiophene) Modified Electrode. *Electroanalysis* 2013, 25, 2244–2250. [CrossRef]
- 23. Zhou, H.; Wang, J.; Yea, B. Electrochemical Investigation of Redox Reactions of Herbal Drug-Shikonin and Its Determination in Pharmaceutical Preparations. *J. Anal. Chem.* **2010**, *65*, 749–754. [CrossRef]
- 24. Gao, Y.-S.; Wu, L.-P.; Zhang, K.-X.; Xu, J.-K.; Lu, L.-M.; Zhu, X.-F.; Wu, Y. Electroanalytical Method for Determination of Shikonin Based on the Enhancement Effect of Cyclodextrin Functionalized Carbon Nanotubes. *Chinese Chem. Lett.* **2015**, *26*, 613–618. [CrossRef]
- 25. An, J.; Li, J.; Chen, W.; Yang, C.; Hu, F.; Wang, C. Electrochemical Study and Application on Shikonin at Poly(Diallyldimethylammonium Chloride) Functionalized Graphene Sheets Modified Glass Carbon Electrode. *Chem. Res. Chinese Univ.* **2013**, 29, 798–805. [CrossRef]
- 26. Hahn, Y.; Lee, H.Y. Electrochemical Behavior and Square Wave Voltammetric Determination of Doxorubicin Hydrochloride. *Arch. Pharm. Res.* **2004**, *27*, 31–34. [CrossRef]
- 27. Abhishek Singh, T.; Sharma, V.; Thakur, N.; Tejwan, N.; Sharma, A.; Das, J. Selective and Sensitive Electrochemical Detection of Doxorubicin via a Novel Magnesium Oxide/Carbon Dot Nanocomposite Based Sensor. *Inorg. Chem. Commun.* **2023**, *150*, 110527. [CrossRef]
- 28. Skalová, Š.; Langmaier, J.; Barek, J.; Vyskočil, V.; Navrátil, T. Doxorubicin Determination Using Two Novel Voltammetric Approaches: A Comparative Study. *Electrochim. Acta* **2020**, 330, 135180. [CrossRef]
- 29. Hashemzadeh, N.; Hasanzadeh, M.; Shadjou, N.; Eivazi-Ziaei, J.; Khoubnasabjafari, M.; Jouyban, A. Graphene Quantum Dot Modified Glassy Carbon Electrode for the Determination of Doxorubicin Hydrochloride in Human Plasma. *J. Pharm. Anal.* **2016**, *6*, 235–241. [CrossRef]
- 30. Karimi-Maleh, H.; Alizadeh, M.; Orooji, Y.; Karimi, F.; Baghayeri, M.; Rouhi, J.; Tajik, S.; Beitollahi, H.; Agarwal, S.; Gupta, V.K.; et al. Guanine-Based DNA Biosensor Amplified with Pt/SWCNTs Nanocomposite as Analytical Tool for Nanomolar Determination of Daunorubicin as an Anticancer Drug: A Docking/Experimental Investigation. *Ind. Eng. Chem. Res.* **2021**, 60, 816–823. [CrossRef]
- 31. Ayla, S.S.; Bahar, H.; Yavuz, S.; Hazer, B.; Ibis, C. The Synthesis and Characterization of Novel Quinone–Amine Polymers from the Reactions of 2,3-Dichloro-1,4-Naphthoquinone and Polyoxypropylenediamines. *Phosphorus. Sulfur. Silicon Relat. Elem.* **2016**, 191, 438–443. [CrossRef]
- 32. Ibis, C.; Ayla, S.S.; Asar, H. Synthesis and Spectral and Electrochemical Characterization of Novel Substituted 1,4-Naphthoquinone Derivatives. *Synth. Commun.* **2014**, *44*, 121–126. [CrossRef]
- 33. Brun, M.-P.; Braud, E.; Angotti, D.; Mondésert, O.; Quaranta, M.; Montes, M.; Miteva, M.; Gresh, N.; Ducommun, B.; Garbay, C. Design, Synthesis, and Biological Evaluation of Novel Naphthoquinone Derivatives with CDC25 Phosphatase Inhibitory Activity. *Bioorg. Med. Chem.* 2005, 13, 4871–4879. [CrossRef] [PubMed]
- 34. Tandon, V.K.; Maurya, H.K.; Kumar, S.; Rashid, A.; Panda, D. Synthesis and Evaluation of 2-Heteroaryl and 2,3-Diheteroaryl-1,4-Naphthoquinones That Potently Induce Apoptosis in Cancer Cells. *RSC Adv.* **2014**, *4*, 12441–12447. [CrossRef]
- 35. de Oliveira, J.C.; Abreu, B.U.; Paz, E.R.S.; Almeida, R.G.; Honorato, J.; Souza, C.P.; Fantuzzi, F.; Ramos, V.F.S.; Menna-Barreto, R.F.S.; Araujo, M.H.; et al. SuFEx-Functionalized Quinones via Ruthenium-Catalyzed C–H Alkenylation: A Potential Building Block for Bioactivity Valorization. *Chem. An Asian J.* 2024, e202400757. [CrossRef]
- 36. Bhand, S.; Patil, R.; Shinde, Y.; Lande, D.N.; Rao, S.S.; Kathawate, L.; Gejji, S.P.; Weyhermüller, T.; Salunke-Gawali, S. Tautomerism in O-Hydroxyanilino-1,4-Naphthoquinone Derivatives: Structure, NMR, HPLC and Density Functional Theoretic Investigations. *J. Mol. Struct.* **2016**, 1123, 245–260. [CrossRef]
- 37. Liang, D.; Streefkerk, D.E.; Jordaan, D.; Wagemakers, J.; Baggerman, J.; Zuilhof, H. Silicon-Free SuFEx Reactions of Sulfonimidoyl Fluorides: Scope, Enantioselectivity, and Mechanism. *Angew. Chemie* **2020**, *132*, 7564–7570. [CrossRef]
- 38. Poroikov, V.V.; Filimonov, D.A. How to Acquire New Biological Activities in Old Compounds by Computer Prediction. *J. Comput. Aided. Mol. Des.* **2002**, *16*, 819–824. [CrossRef]
- 39. Benites, J.; Valderrama, J.A.; Bettega, K.; Pedrosa, R.C.; Calderon, P.B.; Verrax, J. Biological Evaluation of Donor-Acceptor Aminonaphthoquinones as Antitumor Agents. *Eur. J. Med. Chem.* **2010**, *45*, 6052–6057. [CrossRef]
- 40. Doogue, M.P.; Polasek, T.M. The ABCD of Clinical Pharmacokinetics. Ther. Adv. Drug Saf. 2013, 4, 5–7. [CrossRef]
- 41. Daina, A.; Michielin, O.; Zoete, V. SwissADME: A Free Web Tool to Evaluate Pharmacokinetics, Drug-Likeness and Medicinal Chemistry Friendliness of Small Molecules. *Sci. Rep.* **2017**, *7*, 42717. [CrossRef] [PubMed]
- 42. Wellington, K.W.; Kolesnikova, N.I.; Hlatshwayo, V.; Saha, S.T.; Kaur, M.; Motadi, L.R. Anticancer Activity, Apoptosis and a Structure–Activity Analysis of a Series of 1,4-Naphthoquinone-2,3-Bis-Sulfides. *Invest. New Drugs* 2020, 38, 274–286. [CrossRef] [PubMed]
- 43. Randall, J.D.; Eyckens, D.J.; Stojcevski, F.; Francis, P.S.; Doeven, E.H.; Barlow, A.J.; Barrow, A.S.; Arnold, C.L.; Moses, J.E.; Henderson, L.C. Modification of Carbon Fibre Surfaces by Sulfur-Fluoride Exchange Click Chemistry. *ChemPhysChem* 2018, 19, 3176–3181. [CrossRef] [PubMed]
- 44. Andrada, D.M.; Holzmann, N.; Hamadi, T.; Frenking, G. Direct estimate of the internal π-donation to the carbene centre within N-heterocyclic carbenes and related molecules. *Beilstein J. Org. Chem.* **2015**, *11*, 2727–2736. [CrossRef]

45. Lin, Y.-S.; Li, G.-D.; Mao, S.-P.; Chai, J.-D. Long-Range Corrected Hybrid Density Functionals with Improved Dispersion Corrections. *J. Chem. Theory Comput.* **2013**, *9*, 263–272. [CrossRef]

- 46. Verrax, J.; Beck, R.; Dejeans, N.; Glorieux, C.; Sid, B.; Rozangela, C.P.; Julio, B.; David, V.; Jaime, A.V.; Pedro, B.C. Redox-Active Quinones and Ascorbate: An Innovative Cancer Therapy That Exploits the Vulnerability of Cancer Cells to Oxidative Stress. *Anticancer. Agents Med. Chem.* **2011**, *11*, 213–221. [CrossRef]
- 47. Heyrovský, J. Principles of Polarography; Academic Press: New York, NY, USA, 1966.
- 48. Compton, R.G.; Laborda, E.; Ward, K.R. *Understanding Voltammetry: Simulation of Electrode Processes*; Imperial College Press: London, UK, 2013; ISBN 978-1-78326-323-3.
- 49. Gamboa-Valero, N.; Astudillo, P.D.; González-Fuentes, M.A.; Leyva, M.A.; Rosales-Hoz, M.D.J.; González, F.J. Hydrogen Bonding Complexes in the Quinone-Hydroquinone System and the Transition to a Reversible Two-Electron Transfer Mechanism. *Electrochim. Acta* 2016, 188, 602–610. [CrossRef]
- 50. Bailey, S.I.; Ritchie, I.M. A Cyclic Voltammetric Study of the Aqueous Electrochemistry of Some Quinones. *Electrochim. Acta* **1985**, 30, 3–12. [CrossRef]
- 51. Sangeetha, K.; Abraham, T.E. Chemical Modification of Papain for Use in Alkaline Medium. *J. Mol. Catal. B Enzym.* **2006**, 38, 171–177. [CrossRef]
- 52. Rani, S.K.; Easwaramoorthy, D.; Bilal, I.M.; Palanichamy, M. Studies on Mn(II)-Catalyzed Oxidation of α-Amino Acids by Peroxomonosulphate in Alkaline Medium-Deamination and Decarboxylation: A Kinetic Approach. *Appl. Catal. A Gen.* **2009**, 369, 1–7. [CrossRef]
- 53. Tandon, V.K.; Maurya, H.K.; Mishra, N.N.; Shukla, P.K. Design, Synthesis and Biological Evaluation of Novel Nitrogen and Sulfur Containing Hetero-1,4-Naphthoquinones as Potent Antifungal and Antibacterial Agents. *Eur. J. Med. Chem.* **2009**, *44*, 3130–3137. [CrossRef] [PubMed]
- 54. Ishikawa, T.; Eguchi, Y.; Igarashi, M.; Okajima, T.; Mita, K.; Yamasaki, Y.; Sumikura, K.; Okumura, T.; Tabuchi, Y.; Hayashi, C.; et al. Synthesis and Biochemical Characterization of Naphthoquinone Derivatives Targeting Bacterial Histidine Kinases. *J. Antibiot.* 2024, 77, 522–532. [CrossRef] [PubMed]
- 55. Becke, A.D. Density-Functional Exchange-Energy Approximation with Correct Asymptotic Behavior. *Phys. Rev. A* **1988**, 38, 3098–3100. [CrossRef] [PubMed]
- 56. Weigend, F.; Ahlrichs, R. Balanced Basis Sets of Split Valence, Triple Zeta Valence and Quadruple Zeta Valence Quality for H to Rn: Design and Assessment of Accuracy. *Phys. Chem. Chem. Phys.* **2005**, *7*, 3297. [CrossRef] [PubMed]
- 57. Weigend, F. Accurate Coulomb-Fitting Basis Sets for H to Rn. Phys. Chem. Chem. Phys. 2006, 8, 1057. [CrossRef]
- 58. Grimme, S.; Ehrlich, S.; Goerigk, L. Effect of the Damping Function in Dispersion Corrected Density Functional Theory. *J. Comput. Chem.* **2011**, 32, 1456–1465. [CrossRef]
- 59. Neese, F.; Wennmohs, F.; Hansen, A.; Becker, U. Efficient, Approximate and Parallel Hartree–Fock and Hybrid DFT Calculations. A 'Chain-of-Spheres' Algorithm for the Hartree–Fock Exchange. *Chem. Phys.* **2009**, *356*, 98–109. [CrossRef]
- 60. Izsák, R.; Neese, F. An Overlap Fitted Chain of Spheres Exchange Method. J. Chem. Phys. 2011, 135. [CrossRef]
- 61. Khristunova, E.; Barek, J.; Kratochvil, B.; Korotkova, E.; Dorozhko, E.; Vyskocil, V. Electrochemical Immunoassay for the Detection of Antibodies to Tick-Borne Encephalitis Virus by Using Various Types of Bioconjugates Based on Silver Nanoparticles. *Bioelectrochemistry* 2020, 135, 107576. [CrossRef]
- 62. Bard, A.J.; Larry, R. Faulkner, Electrochemical Methods: Fundamentals and Applications; Wiley: Hoboken, NJ, USA, 2000; ISBN 978-0-471-04372-0.
- 63. Herrera Hernández, H.; Ruiz Reynoso, A.M.; Trinidad González, J.C.; González Morán, C.O.; Miranda Hernández, J.G.; Mandujano Ruiz, A.; Morales Hernández, J.; Orozco Cruz, R. Electrochemical Impedance Spectroscopy (EIS): A Review Study of Basic Aspects of the Corrosion Mechanism Applied to Steels. In *Electrochemical Impedance Spectroscopy*; IntechOpen: London, UK, 2020. [CrossRef]

Disclaimer/Publisher's Note: The statements, opinions and data contained in all publications are solely those of the individual author(s) and contributor(s) and not of MDPI and/or the editor(s). MDPI and/or the editor(s) disclaim responsibility for any injury to people or property resulting from any ideas, methods, instructions or products referred to in the content.